Tissue crosstalk during lung development and disease

By

Randee E. Young

A dissertation submitted in partial fulfillment of

the requirements for the degree of

Doctor of Philosophy

(Genetics)

at the

UNIVERSITY OF WISCONSIN-MADISON

2021

Date of final oral examination: 05/24/2021

The dissertation is approved by the following members of the Final Oral Committee:

Xin Sun, Professor, Pediatrics, University of California, San Diego
Barak Blum, Assistant Professor, Cell & Regenerative Biology
Akihiro Ikeda, Professor, Medical Genetics
Francisco Pelegri, Professor, Genetics
Deneen Wellik, Professor, Cell & Regenerative Biolog

Acknowledgements

First and foremost I am extremely grateful to my advisor, Xin Sun, for her invaluable advice and continuous support during the course of my PhD. Xin's immense knowledge, enthusiasm, and deep generosity to all those she mentors has encouraged me and enabled me to succeed during the course of my graduate research. I would also like to thank my committee members Barak Blum, Akihiro Ikeda, Francisco Pelegri, and Deneen Wellik, as well as my past committee members Kate O'Connor-Giles and Ahna Skop, for their suggestions and insight.

Thank you to my lab mates, past and present: Jamie Verheyden, Rongbo Li, Yujuan Su, Jamie Barr, Le Xu, Barsha Dash, Vincent Yu, Albert Xu, Michael Valdez, Gidsela Luna, Estelle Kim, Sunyoung Lee, Abigail Jaquish, Pengfei Sui, Amber Lashua, Leah Nantie, Tina Zhang, Wyatt Paltzer, Chunting Tan, and David McCulley.

I would like to thank the National Science Foundation Graduate Research Fellowship Program and the National Institute of Health Genetics Training Grant for supporting my research.

Finally, I would like to thank my family, including my parents, my sister, and my in-laws, for all of their support and encouragement throughout graduate school. I am particularly grateful to my husband, Sean, whose unwavering support and partnership has been critical during my graduate career.

Table of Contents

Abstract

Developmental biology is a fundamental discipline that explores the universal human experience of embryogenesis, and the building, maintenance, and regeneration of functional tissues. Given the common occurrence of developmental anomalies and congenital disorders, understanding the genetic mechanisms that underly developmental programs is essential to improving human health. Here, I focus my efforts on an organ that is critical for all terrestrial life from the first breath – the respiratory system.

The primary function of the respiratory tissues is to perform efficient gas exchange between the blood and external environment. To achieve this critical goal, the development of the lungs begins early during embryogenesis and continues after birth into post-natal life. During development, endoderm and mesoderm derived tissues become spatially organized into several integrated compartments. These distinct regions of the respiratory tract are composed of unique cell types that include epithelial, endothelial, mesenchymal, and immune cells. It is critical that efficient crosstalk between these diverse cell types are maintained in order for this elaborate organ to achieve its vital function. My graduate studies have focused on uncovering the mechanisms underlying tissue crosstalk during lung development and disease.

Branching morphogenesis is a key stage of early lung development. During branching, the airways of the lung develop into their tree-like structures and establish millions of epithelial tips that each act as a gas exchange unit. As epithelial buds branch, they are in close association with the mesenchyme and the interaction between the epithelium and mesenchyme is fundamental to successful lung development. My

first efforts have focused on a controversial relationship between one key mesenchymal cell type, airway smooth muscle, and it's influence on lung epithelium development. By inactivating *Myocardin*, a transcription factor that is essential for smooth muscle cell fate, we discover that airway smooth muscle plays a complex role during lung development. While it is essential for proper development of tracheal architecture and establishing the size of the pulmonary airways, airway smooth muscle is dispensable for epithelial branching morphogenesis.

After development is complete, the adult lung must maintain homeostasis while constantly experiencing environmental harms including pollutants, toxins, microbes, and allergens that pass through the airways during respiration. The airways serve an important role as the first line of host defense by creating a barrier between environmental insults and the underlying lung tissues. In order for the barrier to function properly, airway epithelial differentiation and communication with the immune system must be properly maintained. The second half of my graduate research has focused on uncovering molecular mechanisms that mediate crosstalk between the airway epithelium and the immune system. By inactivating *E-cadherin* in specific airway epithelial cells, we discover a role for pulmonary club cells in maintaining the airway microenvironment and securing lung homeostasis.

Chapter I: Introduction

The case for developmental biology

Congenital anomalies are common, occurring in 2-3% of infants and are the leading cause of infant deaths [1,2]. While the number of infant mortalities attributable to birth defects has been declining, the proportion of deaths caused by congenital anomalies has remained consistently high for at least the past 40 years, accounting for 30.6% of all infant deaths in 2019 [1,3–5]. It is estimated that around 20% of birth defects are caused by genetic factors [6]. Genetic disorders range from structural or chromosomal anomalies to monogenic disorders. While genetic anomalies are individually rare, they are collectively common and disproportionately contribute to national and global morbidity and mortality [7,8]. It is therefore of great interest to understand the underlying etiologies of congenital abnormalities and developmental disorders.

Genetic mechanisms integral to the development of an embryo are remarkedly conserved across vertebrate species. Advances in developmental biology and genetic discoveries in model organisms have transformed the study of human birth defects. Scientists have long utilized the powerful genetic tools available in model organisms to mechanistically inform how genetics influence not only human development, but human disease. Recent advances in sequencing technology have increased the pace of gene discovery. However, the gap between gene discovery and mechanistic insights provided by studies in model systems has increasingly grown [9]. Developmental biologist are uniquely positioned to link biological science to the fundamental human curiosity of how we, as embryos, built ourselves.

Basic lung development and function

The lung is an organ that is critical for life at the first breath. It is the background for many pediatric and adult diseases where pathogenesis is unknown and few treatments and cures are available. Respiratory disorders, including congenital lung defects and chronic respiratory diseases, impose an immense health burden and are leading causes of death and disability worldwide [10,11]. To improve human health, it is critical to understand the basic mechanisms governing lung development and disease.

The mammalian respiratory system is comprised of the trachea and lungs. The building of the lung begins early during embryogenesis and continues after birth into post-natal life, and is marked by several distinct morphogenetic steps [12]. The earliest known specification of the respiratory lineage occurs at embryonic day 9.0 (E9.0) in mice and approximately embryonic day 28 in humans, when the primary lung buds separate from the anterior foregut [13]. Once the primary lung buds have formed they undergo branching morphogenesis, which initiates at E12 in mice and week 4 of human gestation, and is responsible for generating the tree-like structure of the lung airways [14,15]. Following branching, the lungs undergo sacculation and alveologenesis to form the alveolar epithelium where gas exchange will eventually take place. Alveologenesis begins shortly before birth, and extends into post-natal life until approximately post-natal day 39 in mice and 2 years of age in humans [14,16].

The primary function of the lungs is to perform efficient gas exchange between the blood and external environment. To achieve this critical goal, the respiratory system is comprised of multiple tissues that are spatially organized into several integrated compartments. These distinct regions of the respiratory tract are composed of unique

cell types that include epithelial, endothelial, mesenchymal, and immune cells. It is critical that efficient crosstalk between these diverse cell types are maintained in order for this elaborate organ to achieve its vital function. While there are several differences between mouse and human lung architecture and cellular composition, they are remarkedly similar in their developmental programs, regional specifications, and disease pathogenesis, making mice an excellent model system to understand the underlying mechanisms of lung development and disease.

Lung branching morphogenesis

Branching morphogenesis is a central process in the building of functional tissues in many species: from the stems of plants, to the tracheal system in Drosophila, to animal organs. The iterative, stereotypic process of branching morphogenesis is responsible for defining the architecture of several mammalian organs, including the nervous system, the kidneys and vasculature, and the respiratory system [17]. In the lung, branching morphogenesis maximizes the surface area for gas exchange by establishing millions of epithelial tips that each act as a gas exchange unit [15]. Branching is mediated through reciprocal interactions between the respiratory epithelium and the underlying mesenchyme [18]. As epithelial buds elongate and branch into the surrounding mesenchyme, a diverse pool of mesenchymal progenitor cells differentiates into several cell types including airway and vascular smooth muscle. The close interaction between the epithelium and the mesenchyme are a major driving force of lung branching, and this tissue crosstalk is mediated by several developmental signaling pathways including FGF, BMP, and Hedgehog signaling [19–22].

Aberrations in the interactions between these tissues can lead to severe lung defects that are incompatible with life. Despite the importance of this relationship, it is still unclear what exact roles the mesenchyme plays during lung development – including physical signals from the mesenchyme to guide the branching epithelium or the genetic cues it elicits to control epithelial development. With emerging evidence suggesting that key developmental processes are reactivated upon postnatal injury and repair, elucidating the intricacies of proper lung formation will be important for understanding human lung diseases [23].

Airway epithelial differentiation and regeneration

Pulmonary epithelial differentiation coincides with the termination of branching morphogenesis. As the lung epithelium takes its shape, it also begins to develop into distinct cell lineages along a proximal – distal axis. This regional patterning is marked by *Sox2* expression in the proximal epithelial progenitors, and *Sox9* and *Id2* co-expression in the distal epithelial progenitors [24,25]. These proximal and distal progenitors become restricted to specialized cell fates – the proximal epithelium is composed of airway basal, club, ciliated, mucosal, and pulmonary neuroendocrine cells while the distal epithelium is composed of the alveolar type 1 and type 2 cells [26–28]. The proper maintenance and differentiation of these regionally specific epithelial cell types is important for normal lung function during development and adult homeostasis.

The trachea and proximal airways of mice, and humans, are lined by a pseudostratified epithelium that consists of multiple cell lineages. These proximal airways uniquely contain basal cells, which are restricted to the cartilaginous airways. In

mice the cartilaginous airways are comprised of the trachea and extrapulmonary bronchi, while in humans they also include the large intrapulmonary airways. In mice, basal cells are present early in development at E10.5 and are marked by the transcription factor *Trp63*. Basal cells are multipotent, and serve as progenitors for the airways by giving rise to club, ciliated, and goblet cells [29,30]. Club cells are secretory cells of the airway that are important for hydrating and detoxifying the air, while ciliated cells produce motile cilia to help clear obstructions and mucus from the airway lumen. The earliest known marker of the club cell lineage is *Scgb3a2* which emerges at E11.5, while the earliest presence of ciliated cells at E14.5 is marked the expression of the transcription factor *Foxj1* [31,32]. Notch signaling is critical for maintaining the balance of club and ciliated cells during airway development and regeneration. Notch signaling is required for club cell differentiation, and loss of Notch leads to an overabundance of ciliated cells and the absence of club cells in the airways [33]. Conversely, activation of Notch leads to aberrant goblet cell differentiation which is associated with increased mucus production in the airways [34,35].

Club cells play a central role during lung injury repair and regeneration in adult airways. In homeostasis the adult lung is fairly quiescent with slow cell turnover and low cellular proliferation, but responds to injury with robust regeneration. The adult mouse intrapulmonary airways are absent of basal cells, and club cells serve as the progenitors for ciliated and goblet cells in response to injury and environmental cues. Goblet cell differentiation is induced by toxins, allergens, pathogens, and innate immune signaling. Goblet cells also influence lung responses to environmental stimuli by expression of cytokines and chemokines that recruit immune cells [36]. Goblet cell metaplasia is a

common response to airway injury and a characteristic feature of Th2 immune responses typically seen in asthma.

The airways, like the skin, are in direct contact with the external environment and are constantly exposed to inhaled challenges including microbes, particulate matter, and allergens. The airways form a continuous barrier between the environment and the underlying tissue. The diverse cell types of the airway epithelium act as part of the innate immune system and serve as the first line of host defense for the lungs. There is increasing evidence that disturbances of the airway epithelium may act as a driver for pathogenesis, particularly of allergic airway inflammation [37–39]. Many lung diseases, including asthma and chronic obstructive pulmonary disease (COPD), exhibit dysfunctional airways with heightened immune responses. Understanding how the airway epithelium senses environmental challenges and elicits an immune response is critical to understanding the underlying pathology of airway diseases.

References

1. Centers for Disease Control and Prevention. Web-based Injury Statistics Query and Reporting System (WISQARS). National Center for Injury Prevention and Control, Centers for Disease Control and Prevention. www.cdc.gov/ncipc/wisqars. Published 2020. Accessed May 1, 2021.
2. Wallingford JB. We Are All Developmental Biologists. *Dev Cell*. 2019;50(2):132-137. doi:10.1016/j.devcel.2019.07.006
3. Ely DM DA. Infant mortality in the United States: data from the period linked birth/infant death file. *Natl Vital Stat Rep*. 2019;68:1-19.
4. Petrini J, Damus K JR. Trends in infant mortality attributable to birth defects—United States, 1980–1995. *MMWR Morb Mortal Wkly Rep*. 1998;47:773-778.
5. Lee K, Khoshnood B, Chen L, Wall SN, Cromie WJ MR. Infant mortality from congenital malformations in the United States, 1970–1997. *Obs Gynecol*. 2001;98:620-627.
6. Cleveland Clinic. Birth Defects. https://my.clevelandclinic.org/health/diseases/12230-birth-defects. Accessed May 3, 2021.
7. Xu JQ, Murphy S, Kochanek KD AE. *Mortality in the United States, 2018. NCHS Data Brief, No 355.* Hyattsville, MD; 2020.
8. Boyle B, Addor MC, Arriola L, Barisic I, Bianchi F, Csáky-Szunyogh M, de Walle HEK, Dias CM, Draper E GM et al. Estimating Global Burden of Disease due to congenital anomaly: an analysis of European data. *Arch Dis Child Fetal Neonatal Ed*. 2018;103:F22-F28.

9. Leslie EJ. Embracing human genetics: A primer for developmental biologists. *Dev*. 2020;147(21). doi:10.1242/DEV.191114

10. The Global Impact of Respiratory Disease – Second Edition. Presented at the: 2017.

11. Dwyer-Lindgren L, Bertozzi-Villa A, Stubbs RW et al. Trends and Patterns of Differences in Chronic Respiratory Disease Mortality Among US Counties, 1980-2014. *JAMA - J Am Med Assoc*. 2017;318(12):1136-1149. doi:doi:10.1001/jama.2017.11747

12. Morrisey EE, Hogan BLMM. Preparing for the First Breath: Genetic and Cellular Mechanisms in Lung Development. *Dev Cell*. 2010;18(1):8-23. doi:10.1016/j.devcel.2009.12.010

13. Cardoso W V. Regulation of early lung morphogenesis: questions, facts and controversies. *Development*. 2006;133(9):1611-1624. doi:10.1242/dev.02310

14. Nikolić MZ, Sun D, Rawlins EL. Human lung development: recent progress and new challenges. *Development*. 2018;145(16). doi:10.1242/dev.163485

15. Metzger RJ, Klein OD, Martin GR, Krasnow MA. The branching programme of mouse lung development. *Nature*. 2008;453(7196):745-750. doi:10.1038/nature07005

16. Mund SI, Stampanoni M, Schittny JC. Developmental alveolarization of the mouse lung. *Dev Dyn*. 2008;237(8):2108-2116. doi:10.1002/dvdy.21633

17. Ochoa-Espinosa A, Affolter M. Branching Morphogenesis: From Cells to Organs and Back. *Cold Spring Harb Perspect Biol*. 2012;4(10):a008243-a008243. doi:10.1101/cshperspect.a008243

18. Chuang PT, McMahon AP. Branching morphogenesis of the lung: New molecular insights into an old problem. *Trends Cell Biol*. 2003;13(2):86-91. doi:10.1016/S0962-8924(02)00031-4

19. Bellusci S, Grindley J, Emoto H, Itoh N, Hogan BL. Fibroblast growth factor 10 (FGF10) and branching morphogenesis in the embryonic mouse lung. *Development*. 1997;124(23):4867-4878.

20. Weaver M, Dunn NR, Hogan BLM. Bmp4 and Fgf10 play opposing roles during lung bud morphogenesis. *Development*. 2000;127:2695-2704.

21. Pepicelli C V, Lewis PM, McMahon a P. Sonic hedgehog regulates branching morphogenesis in the mammalian lung. *Curr Biol*. 1998;8:1083-1086. doi:10.1016/S0960-9822(98)70446-4

22. McCulley D, Wienhold M, Sun X. The pulmonary mesenchyme directs lung development. *Curr Opin Genet Dev*. 2015;32:98-105. doi:10.1016/j.gde.2015.01.011

23. Morrisey EE, Cardoso W V., Lane RH, et al. Molecular determinants of lung development. *Ann Am Thorac Soc*. 2013;10(2). doi:10.1513/AnnalsATS.201207-036OT

24. Alanis DM, Chang DR, Akiyama H, Krasnow MA, Chen J. Two nested developmental waves demarcate a compartment boundary in the mouse lung. *Nat Commun*. 2014;(May):1-15. doi:10.1038/ncomms4923

25. Herriges M, Morrisey EE. Lung development: Orchestrating the generation and regeneration of a complex organ. *Dev*. 2014;141(3):502-513. doi:10.1242/dev.098186

26. Que J, Luo X, Schwartz RJ, Hogan BLM. Multiple roles for Sox2 in the developing and adult mouse trachea. *Development*. 2009;136(11):1899-1907. doi:10.1242/dev.034629

27. Rawlins EL, Clark CP, Xue Y, Hogan BLM. The Id2+ distal tip lung epithelium contains individual multipotent embryonic progenitor cells. *Development*. 2009;136(22):3741-3745. doi:10.1242/dev.037317

28. Tompkins DH, Besnard V, Lange AW, et al. Sox2 is required for maintenance and differentiation of bronchiolar Clara, ciliated, and goblet cells. *PLoS One*. 2009;4(12). doi:10.1371/journal.pone.0008248

29. Yang Y, Riccio P, Schotsaert M, et al. Spatial-Temporal Lineage Restrictions of Embryonic p63+ Progenitors Establish Distinct Stem Cell Pools in Adult Airways. *Dev Cell*. 2018;44(6):752-761.e4. doi:10.1016/j.devcel.2018.03.001

30. Rock JR, Onaitis MW, Rawlins EL, et al. Basal cells as stem cells of the mouse trachea and human airway epithelium. *Proc Natl Acad Sci U S A*. 2009;106(31):12771-12775. doi:10.1073/pnas.0906850106

31. Guha A, Vasconcelos M, Cai Y, et al. Neuroepithelial body microenvironment is a niche for a distinct subset of Clara-like precursors in the developing airways. *Proc Natl Acad Sci*. 2012;109(31):12592-12597. doi:10.1073/pnas.1204710109

32. Rawlins EL, Ostrowski LE, Randell SH, Hogan BLM. Lung development and repair: Contribution of the ciliated lineage. *Proc Natl Acad Sci U S A*. 2007;104(2):410-417. doi:10.1073/pnas.0610770104

33. Tsao P-N, Vasconcelos M, Izvolsky KI, Qian J, Lu J, Cardoso W V. Notch signaling controls the balance of ciliated and secretory cell fates in developing

airways. *Development*. 2009;136(13):2297-2307. doi:10.1242/dev.034884

34. Guseh JS, Bores SA, Stanger BZ, et al. Notch signaling promotes airway mucous metaplasia and inhibits alveolar development. *Development*. 2009;136(10):1751-1759. doi:10.1242/dev.029249

35. Zepp JA, Morrisey EE. Cellular crosstalk in the development and regeneration of the respiratory system. *Nat Rev Mol Cell Biol*. 2019;20(9):551-566. doi:10.1038/s41580-019-0141-3

36. Whitsett JA, Kalin T V., Xu Y, Kalinichenko V V. Building and regenerating the lung cell by cell. *Physiol Rev*. 2019;99(1):513-554. doi:10.1152/physrev.00001.2018

37. Nawijn MC, Hackett TL, Postma DS, van Oosterhout AJM, Heijink IH. E-cadherin: Gatekeeper of airway mucosa and allergic sensitization. *Trends Immunol*. 2011;32(6):248-255. doi:10.1016/j.it.2011.03.004

38. Georas SN, Rezaee F. Epithelial barrier function: At the front line of asthma immunology and allergic airway inflammation. *J Allergy Clin Immunol*. 2014;134(3):509-520. doi:10.1016/j.jaci.2014.05.049

39. Heijink IH, Nawijn MC, Hackett TL. Airway epithelial barrier function regulates the pathogenesis of allergic asthma. *Clin Exp Allergy*. 2014;44(5):620-630. doi:10.1111/cea.12296

Chapter II: Smooth Muscle Differentiation is Essential for Airway Size, Tracheal Cartilage Segmentation, but Dispensable for Epithelial Branching

Randee E. Young[1,3], Mary-Kayt Jones[3], Elizabeth A. Hines[3], Rongbo Li[1], Yongfeng Luo[4], Wei Shi[4], Jamie M. Verheyden[1], Xin Sun[1,2,5]

[1]Department of Pediatrics, University of California-San Diego, La Jolla, CA 92093.

[2]Department of Biological Sciences, University of California-San Diego, La Jolla, CA 92093.

[3]Laboratory of Genetics, Department of Medical Genetics, University of Wisconsin-Madison, Madison, WI 53706.

[4]Developmental Biology and Regenerative Medicine Program, Saban Research Institute, Children's Hospital Los Angeles, Los Angeles, CA 90027.

[5]Lead contact

Co-corresponding Authors: Xin Sun (contact)

Jamie M. Verheyden

This chapter has been published as:

Young RE, Jones MK, Hines EA, Li R, Luo Y, Shi W, Verheyden JM, Sun X. Smooth Muscle Differentiation Is Essential for Airway Size, Tracheal Cartilage Segmentation, but Dispensable for Epithelial Branching. Dev Cell. 2020 Apr 6;53(1):73-85.e5. doi: 10.1016/j.devcel.2020.02.001.

Summary

Airway smooth muscle is best known for its role as an airway constrictor in diseases such as asthma. However, its function in lung development is debated. A prevalent model, supported by in vitro data, posits that airway smooth muscle promotes lung branching through peristalsis and pushing intraluminal fluid to branching tips. Here, we test this model in vivo by inactivating *Myocardin*, which prevented airway smooth muscle differentiation. We found that *Myocardin* mutants show normal branching, despite absence of peristalsis. In contrast, tracheal cartilage, vasculature, and neural innervation patterns were all disrupted. Furthermore, airway diameter is reduced in the mutant, counter to the expectation that the absence of smooth muscle constriction would lead to a more relaxed and thereby wider airway. These findings together demonstrate that during development, while airway smooth muscle is dispensable for epithelial branching, it is integral for building the tracheal architecture and promoting airway growth.

Introduction

Specification of the respiratory tract in mice begins at embryonic day 9 (E9) as marked by the expression of *Nkx2.1*, the earliest known genetic marker of the respiratory lineage [1,2]. By E9.5, the lung primordium initiates as two simple epithelial buds surrounded by mesenchyme. Following elongation of the primary buds, secondary branching ensues in a highly stereotypic pattern until approximately E16 [3,4]. Strong evidence demonstrates that close interaction between the juxtaposed mesenchyme and epithelium is important for lung branching morphogenesis [5].

Shortly after lung budding, diverse cell types emerge in the lung mesenchyme [6]. For example, airway smooth muscle (ASM) can be detected starting at E10.5 as a small population of cells between the two lung buds [7]. As development proceeds, ASM forms tightly packed bundles around the intrapulmonary airway epithelium. By E12.5, airway peristaltic contraction can be observed [8]. It has been hypothesized that ASM contraction drives peristalsis, which in turn is essential for maintaining airway fluid pressure and subsequently promoting lung growth [9].

This hypothesis was tested by manipulating ASM in ex vivo lung explant culture. For example, using pharmacological agents to activate or inhibit FGF signaling, SHH signaling, or L-type Ca^{2+} channels, both tip bifurcation and domain branching were disrupted [10,11]. These results led the authors to conclude that ASM differentiation and/or contraction is crucial for lung branching morphogenesis, thereby supporting the hypothesis. However, this hypothesis has not been tested in vivo.

In contrast to the mouse intrapulmonary airway where ASM fully surrounds the epithelium, ASM is only present in the dorsal side of the trachea in juxtaposition to the

cartilage on the ventral side. This complementary relationship is essential for proper tracheal function, where the contractility of the ASM maintains air pressure at inhalation, and the rigidity of the cartilage prevents tracheal collapse at exhalation. We have shown that this juxtaposition is established early during cell fate specification through crosstalk of the ASM and cartilage lineages [7]. Recent studies showed that at a later stage, defects in ASM organization disrupted cartilage segmentation, suggesting continued crosstalk [12,13].

In this study, we test the requirement of ASM in lung development by preventing ASM differentiation. This is achieved by inactivating *Myocardin* (*Myocd*), which encodes a transcription factor that is necessary for the specification of smooth muscle cell fate [14]. MYOCD binds co-activator serum response factor (SRF), and together they activate expression of key smooth muscle genes including *actin alpha 2* (*Acta2*, also termed alpha smooth muscle actin), and *transgelin* (*TagIn*, also termed *SM22α).* We found that inactivating *Myocd* in the trachea and lung mesenchyme effectively prevented ASM differentiation. Using this mutant, we tested the in vivo role of differentiated ASM in branching morphogenesis and other aspects of lung development.

Results

Myocd inactivation led to loss of airway smooth muscle cells

To determine the specific role of differentiated smooth muscle cells for lung and trachea development, we inactivated *Myocardin* (*Myocd*) in the developing lung and tracheal mesenchyme by generating *Tbx4rtTA;tetOcre;Myocd*$^{flox/flox}$ mutant mice; hereafter referred to as *Myocd*^{CKO} [15,16]. We activated rtTA by doxycycline administration starting at E5.5, which led to widespread cre activity in the lung and trachea mesenchyme at the onset of lung development [15]. At E12.5, shortly after the initiation of secondary branching morphogenesis, there was a clear loss of airway smooth muscle (ASM) cells in the *Myocd*^{CKO} lung by immunostaining as compared to control (Figure 1A,B). Efficient gene inactivation and overall reduction of smooth muscle was confirmed by qRT analysis of *Myocd*, *Acta2* and *Tagln* (Figure 1C). Interestingly, we observed selective loss of ASM while vascular smooth muscle (VSM) remained intact (Figure 1D-G). To determine if the differential requirement for *Myocd* in ASM and VSM is due to its differential expression in these tissues, we visualized *Myocd* transcripts using RNAscope in the E14.5 lung. Compared to robust *Myocd* expression in the ASM, only significantly reduced expression was observed in the VSM (Supplemental Figure 1). As *Tbx4rtTA;tetOcre* is active in both smooth muscle lineages when induced early as we did [15], this suggests that *Myocd* is singularly required for ASM differentiation, but may work with other factors redundantly in the lung VSM.

Lung epithelial branching continued despite disruption of airway smooth muscle differentiation

Myocd^{CKO} mutants died at birth. Lung size and gross morphology appeared normal at E18.5 (Figure S2A, B). To specifically address if ASM is essential for branching morphogenesis in vivo, we carried out either immunofluorescence staining with anti-ACTA2 and anti-CDH1 (also called E-Cadherin, an epithelium marker) antibodies (Figure 2A,B), or immunohistochemical staining with anti-CDH1 antibody at E14.5 (Figure S2C-F). The gross morphology of E14.5 *Myocd*^{CKO} mutants from an independent source and distinct genetic background was also documented (Figure S2G,H). Quantification was carried out by counting the number of epithelial tips from the left lobes of either *Myocd*^{CKO} and controls (N=11 for each). No statistically significant difference was found (Figure 2C).

We also addressed if there is any difference in the pattern of epithelial tips. A previous study defined four stages of bifurcation branching morphogenesis based on epithelial tip morphology [17]. Epithelial buds begin as a single tip in stage one, flatten in stage two, form a cleft in stage three, and bifurcate into two daughter buds in stage four. We quantified the number of tips in each of the four stages of epithelial bifurcation and found no statistical difference between *Myocd*^{CKO} lungs and controls, even though ASM is absent from the epithelial bifurcation clefts (Figure 2D-F). In addition, our quantification indicated that the epithelial bud tip area was not significantly altered in *Myocd*^{CKO} lung compared to controls (Figure 2G). These data together led to the unexpected conclusion that despite severe disruption of ASM differentiation, the

Myocd^{CKO} lungs exhibited normal branching, suggesting that ASM differentiation is not required for branching morphogenesis.

In addition to investigating the role of smooth muscle differentiation, we also determined if smooth muscle contraction is essential for lung branching. *Mylk* (which encodes MLCK, myosin light chain kinase) is essential for ASM contraction in many tissues including when inactivated in the adult lung [18]. When inactivated during development, we found that *Tbx4rtTA;tetOcre;Mylk*$^{fl/fl}$ mutants (*Mylk*^{CKO}) exhibited normal branching pattern, despite a clear loss of MLCK (Figure S2I-L). This result suggests that similar to the finding from the ASM differentiation mutant, ASM contraction is not required for branching morphogenesis.

Loss of airway smooth muscle abrogated airway peristalsis

Airway peristalsis, presumably driven by ASM, has been postulated as a key component of ASM function in branching. To determine if peristalsis was affected in the *Myocd*^{CKO} mutants, we dissected E12.5 lungs and cultured them at air-liquid interface under conditions that have been previously described to preserve peristalsis in the control [8]. At the time of harvest and start of culture, there was no significant difference in overall lung morphology between the *Myocd*^{CKO} and control (Figure 3A,B). We confirmed that after 24 hours in culture, the *Myocd*^{CKO} ex vivo lungs maintained a significant reduction in ASM compared to controls (Figure 3C-F). While control lungs underwent approximately 1$\pm$0.2 peristaltic contractions per minute, the *Myocd*^{CKO} lungs never contracted (Figure 3G, Movie S1, Movie S2). This suggests that airway peristalsis

is dependent on the presence of ASM, and the absence of peristalsis in *Myocd*^{CKO} lungs does not affect branching morphogenesis.

Cartilage segmentation occurs through cell aggregation

Previous findings from our lab showed that the juxtaposition of ASM and cartilage in the trachea is established early in development and crosstalk between cells of these two lineages impact their fate specification [19]. However, the possible effect of ASM on cartilage condensation into segmented rings was not investigated. To begin addressing this question, we first characterized the timing of the wild-type process of cartilage segmentation. By wholemount RNA in situ hybridization of *Col2a1*, a marker for specified cartilage fate, tracheal cartilage cells emerge as a continuous band which start to be segmented at E13.5 (Figure S3A-D). We reasoned that the conversion from a sleeve to a segmented pattern may occur through either selected intersegmental cell death, or intersegmental trans-differentiation into non-cartilage fate, or convergence of cartilage cells into evenly spaced condensations. To distinguish among these possibilities, we first examined cell death. Immunostaining for apoptosis marker cleaved-Caspase 3 (CASP3) showed little cell death in the ventral mesenchyme, suggesting that mesenchymal cell death is unlikely a major contributor (Figure S3E). Next, we performed lineage tracing employing a *Col2a1-cre* to recombine a double reporter allele *Rosa26R-loxp-tdTom-stop-loxp-eGFP* (abbreviated *RmTmG*) [20,21]. This system allowed us to trace the pattern of *Col2a1*-lineaged cells in the cartilage sleeve as they form segments. At E12.5, we observed that GFP expressing *Col2a1-cre* lineage labeled cells were positioned in an unsegmented band in the pre-condensation trachea

before splitting into two bands in the main bronchi (Figure S3F). However, by E16.5, three days after cartilage segmentation, lineage labeled trachea exhibited an alternating pattern of GFP and tdTomato expressing cells (Figure S3G). This pattern persisted after birth (Figure S3H). The lineage tracing data argue against the possibility that some of the cartilage precursors in the continuous sleeve trans-differentiated into non-cartilage fate in the intersegmental region. Instead, these results together suggest that tracheal cartilage segmentation occurs via convergence of cartilage cells into evenly spaced C-shaped rings.

Airway smooth muscle differentiation is essential for proper tracheal architecture

Based on the above analysis, tracheal cartilage segmentation initiates at E13.5, after ASM differentiates and begins its phasic contractions at E11.5 [8,19]. To determine if loss of ASM differentiation in the *Myocd*^{CKO} trachea would affect cartilage segmentation, we first stained E17.5 tracheas with alcian blue to outline the cartilage. The *Myocd*^{CKO} mutant tracheas exhibited a near complete disruption of C-shaped rings, with stained nodules only on the lateral edge of the trachea in a segmented pattern (Figure 4A,B). This defect can be traced to E14.5, at the start of cartilage segmentation, as indicated by *Col2a1* RNA in situ hybridization (Figure 4C,D). On sections, SOX9+ cartilage cells were still present in similar patterns in the control and *Myocd*^{CKO} tracheas at E13.5, the start of cartilage segmentation (Figure 4E,F). After cartilage segmentation, there was a clear reduction of SOX9+ cells at E14.5 in the *Myocd*^{CKO} (Figure 4G,H). By E17.5, the remaining SOX9+ cells were found in nodules at the lateral edge of the ventral portion of the trachea, similar to the pattern of wholemount alcian blue staining (Figure 4I,J).

This severe reduction of cartilage may lead to collapsed trachea, a possible cause for the lethality of the *Myocd*^{CKO} mutants at birth. Consistent with the findings from the *Myocd*^{CKO} mutants, in the *Mylk*^{CKO} trachea where ASM remains present but its contraction was inhibited, tracheal cartilage pattern is disrupted (Figure S4A-D). These findings together indicate that ASM differentiation and contraction are required for tracheal cartilage segmentation.

To determine the molecular mechanism of tracheal cartilage malformation in the absence of ASM, we performed RNA-seq of control and *Myocd*^{CKO} E18.5 tracheas. The significantly downregulated genes in the *Mycod*^{CKO} trachea consisted of genes in the categories of smooth muscle, cartilage, ion channels, neuronal regulation, and immune response (Figure 4K).

To determine possible molecular players mediating ASM effects on cartilage segmentation, we focused on mechanical pressure regulated genes. Previous studies have identified several genes that are regulated by mechanical pressure, and in turn play a role in chondrocytes and osteoblast development and maturation [22,23]. For example, *Runx2* is a transcription factor that is activated during mechanical loading in osteoblasts and is also necessary for chondrocyte maturation. *Runx2* activates *Spp1* and *Itgbl1*, also mechanoresponsive genes expressed in chondrocytes [24,25]. *Hapln1* is an essential component of the cartilage extracellular matrix (ECM), and *Hapln1* mutants die at birth due to impaired tracheal cartilage and subsequent respiratory failure [26]. *Hapln1* also modulates hyaluronic acid signaling which has been shown to be important for mechanical responses in cartilage [25]. *Itgbl1* has been shown to receive input from the ECM [27]. qRT-PCR analysis validated the RNA-seq data that the expression of

mechanosensitive genes such as *Runx2, Spp1, Hapln1,* and *Itgbl1* are downregulated in the *Myocd*^{CKO} trachea compared to control at E18.5 (Figure 4L). However, the caveat is that their downregulation may be due to the significant reduction of SOX9+ cartilage cells at E18.5, as these genes are primarily expressed in the cartilage cells. To more rigorously determine if loss of ASM may affect these mechanosensitive genes, we examined their expression at E13.5, the stage before cartilage segmentation when there is still a comparable abundance of SOX9+ cells in the *Myocd*^{CKO} and control tracheas. We found that while the expression of *Sox9* in the *Myocd*^{CKO} trachea at E13.5 is proportional to control, the expression of *Runx2, Spp1,* and *Hapln1* is already downregulated (Figure 4M). Together, these findings suggest that in the absence of ASM, changes in mechanical pressure would alter the expression of mechanosensitive genes which in turn may affect cartilage segmentation.

To determine if the lack of ASM also affects the development of other cell types in the trachea, we assayed for the morphology of neurons and vessels. By anti-TUBB3 staining, a pan neuronal marker, several ganglia composed of intrinsic neurons are found to be distributed along the length of the dorsal trachea on the surface of smooth muscles (Figure S5A). While ganglia are still present in the *Myocd*^{CKO} trachea, the cumulative cell body size are ~50% the total area of control ganglia (Figure S5B-E). These results suggest that ASM is important for proper tracheal innervation by intrinsic neurons during development.

To assess patterning of the tracheal vasculature, we used anti-ICAM2 staining, a pan endothelial marker. In the control, there is a net-like appearance of vasculature on the dorsal side while there is a striped organization of vasculature interspaced between

the cartilage rings on the ventral side (Figure S5F-I). In the *Myocd*^{CKO} trachea, vascular patterning on the dorsal side appeared normal, while vessels on the ventral side were no longer constrained in stripes in the absence of organized segmental cartilage rings (Figure S5J-M).

Airway smooth muscle is dispensable for the ability of lung epithelial cells to differentiate

The alveolar epithelium is comprised of alveolar epithelial type 1 cells (AT1) which line the alveolus and form the air-blood barrier, and alveolar epithelial type 2 (AT2) cells which secrete surfactants and reduce surface tension. A proper ratio of AT1 to AT2 cells is crucial for postnatal life. By immunostaining and qRT analysis, the number of AT1 and AT2 cells, and their ratio remained similar in *Myocd*^{CKO} lungs at E18.5 compared to control (Figure S6A-D).

For a more comprehensive analysis of changes in *Myocd*^{CKO} lungs, we performed RNA-seq in *Myocd*^{CKO} and control E18.5 lungs. The significantly downregulated genes in the *Mycod*^{CKO} lung consists of genes related to smooth muscle cells, ciliated cells, club cells, and immune response (Figure 5A). By qRT analysis, we verified that the expression of several genes that are key markers of differentiated airway epithelial cell types were significantly downregulated in the *Myocd*^{CKO} lung at E18.5 (Figure 5B). These include *Scgb1a1* and *Scgb3a2* for club cells; *Foxj1*, *Mcidas* and *Myb* for ciliated cells; *Ascl1* and *Calca* for pulmonary neuroendocrine cells.

Counter to the downregulation of airway epithelium marker expression by qRT-PCR, by immunostaining, airway epithelial cell markers such as SCGB1A1 for club cells,

FOXJ1 for ciliated cells and CGRP for pulmonary neuroendocrine cells were detected at a similar intensity per cell in the *Myocd*^{CKO} lung compared to control (Figure 5C-I). We also found that there was no difference in the balanced ratio of club and ciliated cells in either the *Myocd*^{CKO} or *Mylk*^{CKO} compared to respective controls (Figure S6E-J). Additionally, while pulmonary neuroendocrine cells are present and remain innervated, the neuroepithelial cell body clusters were smaller in the *Myocd*^{CKO} airway as compared to control (Figure 5G-I, Figure S6K-N).

Airway smooth muscle promotes airway circumferential growth

To resolve the discrepancy between qRT-PCR and immunostaining results of airway genes, we used immunostaining of thick longitudinal airway sections and 3D reconstruction of confocal images to visualize the entire thickness of the main intrapulmonary airway. Strikingly, the main airway was narrower in the E18.5 *Myocd*^{CKO} lung compared to control, and quantification demonstrated statistical significance (Figure 6A-C). We can trace this phenotype to E14.5 by taking transverse sections of the primary bronchi at equivalent depths in the *Myocd*^{CKO} and control (Figure 6D,E). Cell counting analysis revealed an approximately 40% decrease in the number of SOX2+ epithelial cells and a similar decrease in airway diameter in the *Myocd*^{CKO} compared to control (Figure 6F,G). This is consistent with the decreased level of *Sox2* expression by qRT-PCR analysis (Figure 5B). No change in cell death or apical-basal polarity was detected (Figure S7A-H). In comparison, there is a small, but statistically significant decrease in epithelial cell proliferation, shown by a reduction in the percentage of Ki67+SOX2+ proliferative airway cells in the total SOX2+ airway epithelial cells in the

Myocd^{CKO} airway compared to control (Figure 6H-J). Over time, this modest decrease in proliferation may accumulate and contribute to the clear difference in airway size at E18.5.

To test the possibility that ASM contractions may be necessary for establishing airway epithelial size, we examined airway size in the *Mylk*^{CKO} mutant lung compared to control. We found that there was no airway size defect in the *Mylk*^{CKO} lung, suggesting that differentiated ASM, but not contraction, is necessary for increasing the caliber of the airway tube (Figure S7I-K).

These findings led to the hypothesis that differentiated ASM may be a source of signaling factors that control the size of the airway epithelium. To uncover the molecular mechanism, we performed RNA-seq of *Myocd*^{CKO} and control lungs at E13.5. We focused in on the signaling factors that are altered (Figure 7A). Among them, two key inhibitors of BMP signaling, *Chrdl1* and *Grem2*, were downregulated. These changes stood out because active BMP signaling has been shown to constrain airway proliferation [28]. By qRT-PCR, we verified that the expression of *Chrdl1* and *Grem2* is significantly decreased in the *Myocd*^{CKO} lung at E13.5 (Figure 7B). We analyzed BMP activity using anti-phosphorylated-SMAD1/5/8 (pSMAD1/5/8) immunostaining as a read-out of BMP activity. In concert with the decrease of BMP inhibitors, we observed a robust increase ($p<0.0005$) of pSMAD1/5/8 staining in the E13.5 main airway of the *Myocd*^{CKO} mutant compared to control, demonstrating increased signaling (Figure 7C-G). These findings suggest that differentiated ASM is essential for promoting the circumferential growth of the airway, and differentiated ASM may act through regulating BMP signaling in this process.

Discussion

The ASM is a prominent site of pathogenesis in diseases such as asthma and COPD, and has been studied extensively in the context of pathogenesis. In comparison, its function in normal development is less understood. In this study, we used an in vivo genetic approach to test the role of ASM differentiation in lung development. Unexpectedly, our findings from the *Myocd*^{CKO} challenged the notion that ASM, through its role in peristalsis, is essential for lung branching morphogenesis, a prevalent model supported by in vitro data [8,11,17,29]. Instead, our data showed that disruption of ASM differentiation abolished peristalsis, but did not alter epithelial branching. Nevertheless, ASM differentiation is far from being dispensable. In the trachea, ASM is essential for the establishment of tracheal architecture, including cartilage segmentation, vascular patterning, and intrinsic neuron organization. The changes of these cell types in the mutant are either direct or indirect consequences of the loss of ASM. Given that in human, the juxtaposition of the ASM and cartilage is preserved deep into the lung, this role of ASM in establishing the cartilaginous airway architecture would prove significant in the human airway. An additional finding from the *Myocd*^{CKO} mutant is that the differentiated ASM is required for circumferential growth of the airway. Postnatally in diseases such as asthma, increased number, size, and/or constriction of ASM cells is linked to airway narrowing. These findings suggest distinct roles of ASM in development versus pathogenesis.

The model that ASM is essential for branching morphogenesis follows the logic that differentiated ASM undergoes peristalsis. In the amniotic fluid filled fetal lung, peristalsis

would push fluid into the distal tips to promote epithelial branching morphogenesis. This attractive model is supported by data from in vitro explant cultures. For example, experimentally increasing intraluminal pressure in culture led to increased branching [30]. Furthermore, disruption of ASM in culture via treatment with a series of pharmacological agents each led to disruption of branching [11,17]. We speculate that the discrepancy between these findings versus ours may be due to the difference between in vitro versus in vivo experimental settings. Furthermore, pharmacological agents used in the in vitro experiments have been shown to have effects not restricted to ASM. In our in vivo model, the genetic data demonstrate that even though ASM is lost and peristalsis is absent in the *Myocd*^{CKO} lung, branching is not altered. This finding is consistent with two prior in vivo observations. First, in two separate studies, it was found that infiltration of amniotic fluid into the distal airway was observed starting at E16.5 [31,32]. As branching morphogenesis has largely concluded by E16.5, it is unlikely that in vivo, amniotic fluid pressure on the distal tip would affect branching. Second, it was found that inhibition of retinoic acid signaling in vivo resulted in ectopic ASM differentiation into the distal airway. However, epithelial branching continued as normal [33]. These findings, together with our data from the *Myocd*^{CKO} mutant, suggest that presence and the amount of differentiated ASM and their function in peristalsis do not impact epithelial branching morphogenesis in vivo.

It should be noted that preventing ASM differentiation is a distinct operation from ablating ASM, and may have different impacts on the adjacent epithelium. In a recent study, genetic ablation of ACTA2+ cells was achieved via *Acta2-cre* mediated expression of diphtheria toxin receptor expression and supply of toxin in the ex vivo

culture medium. This did not affect domain branch number or position, but led to reduced branch length and increased width [11]. In the adult lung, after LGR6^{+} ASM cells were genetically ablated, the airway epithelial cells became defective in regeneration following naphthalene induced airway injury [34]. These results are consistent with findings indicating that ASM is a niche and source of growth signals such as FGFs and WNTs for branching and activation of epithelial progenitors in adult injury repair [35–37].

For ASM function in tracheal cartilage segmentation, we hypothesize that this is achieved through mechanical load exerted by ASM constriction. The impact of mechanical force on cartilage formation has been demonstrated in axial and appendage skeletal development. For example, in limb development, mechanical pressure generated by skeletal muscles is essential for shaping the limb cartilage [38,39]. In the trachea, two independent recent studies showed that ASM-targeted inactivation of *Kcnj13* which encodes a potassium channel, or *Ror2* which encodes a WNT5a receptor, led to misalignment of the ASM, which in turn led to disrupted tracheal cartilage segmentation [12,13]. These findings suggest that disruption of tensile strengths of muscle could impair mechanical stability of the trachea and lead to cartilage condensation defects. For a possible molecular mechanism, work in chondrocytes outside of the trachea has demonstrated that mechanical load can regulate the expression of several genes that play key roles in cartilage formation, including *Runx2*, *Spp1,* and *Hapln1* [22–27]. Our data indicate that the expression of these genes is altered in the *Myocd*^{CKO} trachea, consistent with the possibility that these molecular changes may contribute to the observed cartilage malformation.

While prevention of ASM differentiation did not affect branching morphogenesis, it led to an unexpected reduction of airway diameter. Airway diameter is directly proportional to airway conductance, and decreased airway conductance is a key feature of major lung diseases such as asthma. In Asthma, while decrease of airway conductance is largely due to airway constriction and mucus-based occlusion, one would expect that a narrower airway from development would add to the susceptibility to reduced conductance. However, little is known about how airway diameter is achieved through development, partly because many mutants that show abnormal airway diameter also show disrupted branching. The lack of a branching defect in the *Myocd*^{CKO} lung allowed us to clearly demonstrate the airway diameter phenotype. Reduction of airway diameter only affected a small proportion of the whole lung, thereby did not alter overall lung size. Our finding that the reduced diameter is already present at E14.5 suggests that active circumferential growth occurs in parallel to branching morphogenesis.

In asthma, ASM hyperplasia or hypertrophy is linked to reduced airway size. Thus, the lack of differentiated ASM is expected to lead to relaxed, and thereby larger airway. Our finding that the *Myocd*^{CKO} airway is smaller runs counter to expectation, and suggest that the role of ASM in development is distinct from that in the adult airway. We considered the possibility that mechanical force generated by differentiated ASM may be important for the stimulation of airway epithelial growth, similar to its role in cartilage condensation. However, our finding that the *Mylk*^{CKO} lung did not exhibit an airway size defect does not add credence to this possibility. Alternatively, as mentioned above, differentiated ASM is a source of signal and signaling regulators. We found that BMP4

antagonists *Chrdl1* and *Grem2* are significantly downregulated in the *Myocd*^{CKO} lung. Single cell RNA-seq data from embryonic lungs shared on the LungGENS database revealed that *Chrdl1* and *Grem2* are selectively expressed in ASM and proliferative mesenchymal progenitors [40]. Furthermore, *Bmpr1a* and *Bmpr1b*, which encodes BMP receptors, are expressed in airway epithelial cells. The decrease in *Chrdl1* and *Grem2* are consistent with an increase in BMP activity in the proximal airway, as demonstrated by pSMAD staining. BMP signaling has been shown to influence airway and alveolar epithelial repair [28,41,42]. Specifically, BMP constrains the proliferation of airway cells and this can be released by BMP antagonists in the context of airway repair [28,41,42]. Our results suggest the possibility that ASM differentiation promotes airway diameter growth through regulating signaling. Taken together, the in vivo findings in this study revealed unexpected roles of ASM during the building of a functional lung.

Methods

Lead contact and materials availability

Further information and requests for resources and reagents should be directed to and will be fulfilled by the Lead Contact, Xin Sun (xinsun@ucsd.edu). All RNA-seq fastq and processed files are publicly available at the NIH NCBI GEO database accession number GSE143394.

Experimental model and subject details

Myocd^{flox}*, Tbx4rtTA,* and *tetOcre* alleles and transgenic lines have been described previously [15,43]. *Myocd*$^{flox/+}$ mice were bred to *Tbx4rtTA;tetOcre;Myocd*$^{flox/flox}$ to generate trachea and lung mesenchyme specific knockouts. The *Mylk*$^{flox/flox}$ allele has been described previously [44]. *Mylk*$^{flox/flox}$ mice were bred to *Tbx4rtTA;tetOcre;Mylk*$^{flox/+}$ to generate trachea and lung mesenchyme specific knockouts. Mice were housed and all experimental procedures were performed in an American Association for Accreditation of Laboratory Animal Care-accredited laboratory animal facility at the University of California San Diego (UCSD). Noon of the day on which a virginal plug was detected was considered to be E0.5. Prenatal rtTA activity was induced by doxycycline (dox) administration starting at gestational day 5.5 by feeding pregnant females with dox food (625 mg/kg; Test-Diet, Richmond, IN, USA).

Tissue preparation and immunostaining

Whole E12.5, E13.5, E14.5, E17.5, and E18.5 embryos, tracheas, and lungs were fixed in 4% paraformaldehyde (Electron Microscopy Sciences) diluted in PBS. Samples were either stained wholemount or embedded in paraffin or frozen in OCT (Electron Microscopy Sciences) for sectioning. Whole lungs and sections were immunostained using standard protocols. For pSMAD1/5/8 staining, the Tyramide SuperBoost™ Kit (ThermoFisher) was used followed by TrueBlack® Lipofuscin Autofluorescence Quencher (Biotium) staining following these product's published protocols. Slides were mounted with either Vectashield (Vector Labs) and visualized/photographed using a Zeiss AxioImager.A2 microscope and AxioCam MRc camera. Whole mount images and thick cryo sections were mounted using Citifluor (Ted Pella, Inc.) and visualized/photographed using Zeiss 880 Airyscan and/or Leica Sp8 confocal microscopes and cameras. Images were processed using ImageJ.

Quantitative RT-PCR (qRT-PCR)

RNA was isolated from embryonic whole lungs or tracheas using an RNEasy micro kit (Qiagen), respectively, as per the manufacturer's protocol. Either 250µg, 500µg, or 1000µg of RNA was reverse transcribed into cDNA using the iScript Reverse Transcriptase (Bio-Rad Laboratories). For qRT-PCR, 10ng of cDNA was amplified using gene-specific primers and iTaq SYBR green Supermix (Bio-Rad Laboratories) on a Bio-Rad CFX Connect real-time PCR machine. For each gene, at least three technical replicates and three biological replicates were assayed. Data were analyzed with the change in cycle threshold (Ct) value method. Statistical significance was determined

using Student's t-test. For a list of gene-specific primers, see Table S1.

Analysis of peristalsis in *ex vivo* embryonic lungs

Lungs from E12.5 mouse embryos were dissected in sterile PBS and cultured on porous membranes (nucleopore polycarbonate track-etch membrane, 8 mm pore size, 25 mm diameter; Whatman) at air-liquid interphase of DMEM/F12 medium supplemented with antibiotics (50 units/ml of penicillin and streptomycin). *Ex vivo* lungs were cultured in an incubator at 37^{o}C in 5% CO_2 for 24 hours. Cultured lungs were imaged and videoed for 10 mins on a 37^{o}C warm plate. Peristaltic contractions were calculated by observing the most proximal bronchial branch junction in the right lung. After imaging, *ex vivo* cultured lungs were then fixed in 4% paraformaldehyde (Electron Microscopy Sciences) diluted in PBS and immunostained using standard protocols.

RNAscope in situ hybridization

RNAscope Multiplex Fluorescent v2 Assay (ACD) was used to perform in situ hybridization of *Myocd* in E14.5 wild-type lungs. Tissue was prepared as a fresh-frozen sample following the published RNAscope protocol, then sectioned 10 μm thick. The *Myocd* probe was stained with the Opal 520 fluorophore. These sections were then counter stained with DAPI and the ACTA2 antibody as described above.

Whole-Mount in situ hybridization

Embryonic lungs were dissected in PBS, fixed in 4% paraformaldehyde overnight at 4°C, and then dehydrated to 100% MeOH. Whole-mount in situ hybridization was

carried out by using an established protocol [45].

RNA-seq analysis

Control and *Myocd*^{CKO} E13.5 lungs, E18.5 tracheas, and E18.5 lungs were dissected in PBS and immediately stored in TRIzol Reagent (ThermoFisher Scientific). Tissues were then lysed using a TissueLyser (Qiagen), and total mRNA was extracted using standard TRIzol RNA extraction protocol. mRNA was cleaned using the RNeasy Micro Kit (Qiagen). cDNA libraries were made for each individual lung or trachea using Illumina TruSeq RNA Library Prep Kit V2 (Illumina) and sequenced on a SR75 run on the HiSeq4000 platform (Illumina). Sequences in FASTQ files were aligned to the mouse reference genome using STAR [46]. Reads were counted using featureCounts and differential expression analysis was performed using DeSeq2 [47,48]. Heatmaps were generated using HeatMapper software [49].

Quantification and statistical analysis

Cell counts were quantified manually using the ImageJ Cell Counter feature. For each sample, six different sections from the same lung were quantified and the average was taken to represent the count for each sample. Area was also measured in ImageJ. For E14.5 epithelial tips, area was calculated for each tip and the average was taken as the tip area for each left lobe. For tracheal ganglia, the ganglia were measured individually and then added together to represent the total ganglia area per trachea. Airway diameter measurements were measured in ImageJ. For thick sections, diameter was measured by drawing a straight line through the diameter of the main pulmonary

airways and calculating the length. For transverse sections of the circular main airway, diameter was measured by drawing a straight line through the circular airway. For each sample, three different sections from the same lung at similar depths were quantified and the average was taken to represent the diameter for each sample. pSMAD1/5/8 fluorescence activity was measured for the first proximal branches as pixel intensity for the pSMAD1/5/8 channel (green) in the confocal stacks. Statistical significance was determined using Student's t-test, and presented as mean ± standard deviation.

Data and code availability

All RNA-seq fastq and processed files are publicly available at the NIH NCBI GEO database accession number GSE143394.

https://www.ncbi.nlm.nih.gov/geo/query/acc.cgi?acc=GSE143394

Acknowledgements

We thank the members of the Sun lab for insightful discussions. We thank Dr. Michael Parmacek and Dr. Minsheng Zhu for sharing mouse strains. Confocal imaging was performed at the UCSD School of Medicine Microscopy Core, supported by NINDS NS047101. RNA-seq was conducted at the UCSD IGM Core. This work was supported by National Heart, Lung, and Blood Institute grants R01 HL142215, HL143256, HL122406 and HL119946 (to X.S.). R.Y. has received support from the NSF GRFP #DGE-1747503 and the Laboratory of Genetics at U.W. Madison NIH Training Grant #5T32GM007133.

Author Contributions

Conceptualization: R.E.Y., X.S.; Methodology: R.E.Y., J.M.V., X.S.; Validation: R.E.Y.; Formal analysis: R.E.Y., R.L.; Investigation: R.E.Y., M.K.J., E.A.H., R.L., Y.L., W.S.; Resources: R.E.Y., X.S.; Data curation: R.E.Y.; Writing: R.E.Y., X.S.; Visualization: R.E.Y., X.S.; Supervision: X.S.; Project administration: X.S.; Funding acquisition: R.E.Y., X.S.

References

1. Lazzaro D, Price M, Felice D, et al. The transcription factor TTF-1 is expressed at the onset of thyroid and lung morphogenesis and in restricted regions of the foetal brain. *Development*. 1991;113(4):1093-1104.
2. Harris-Johnson KS, Domyan ET, Vezina CM, Sun X. β-Catenin promotes respiratory progenitor identity in mouse foregut. *Proc Natl Acad Sci U S A*. 2009;106(38):16287-16292. doi:10.1073/pnas.0902274106
3. Metzger RJ, Klein OD, Martin GR, Krasnow MA. The branching programme of mouse lung development. *Nature*. 2008;453(7196):745-750. doi:10.1038/nature07005
4. Short K, Hodson M, Smyth I. Spatial mapping and quantification of developmental branching morphogenesis. *Dev*. 2013;140(2):471-478. doi:10.1242/dev.088500
5. Morrisey EE, Hogan BLM. Preparing for the First Breath: Genetic and Cellular Mechanisms in Lung Development. *Dev Cell*. 2010;18(1):8-23. doi:10.1016/j.devcel.2009.12.010
6. Peng T, Tian Y, Boogerd CJ, et al. Coordination of heart and lung co-development by a multipotent cardiopulmonary progenitor. *Nature*. 2013;500(7464):589-592. doi:10.1038/nature12358
7. Hines E a, Jones MN, Verheyden JM, et al. Establishment of smooth muscle and cartilage juxtaposition in the developing mouse upper airways. *Proc Natl Acad Sci U S A*. 2013;110(48):19444-19449. doi:10.1073/pnas.1313223110/-/DCSupplemental.www.pnas.org/cgi/doi/10.1073/pnas.1313223110
8. Schittny JC, Miserocchi G, Sparrow MP. Spontaneous peristaltic airway

contractions propel lung liquid through the bronchial tree of intact and fetal lung explants. *Am J Respir Cell Mol Biol*. 2000;23(1):11-18. doi:10.1165/ajrcmb.23.1.3926

9. Jesudason EC, Smith NP, Connell MG, et al. Peristalsis of airway smooth muscle is developmentally regulated and uncoupled from hypoplastic lung growth. *Am J Physiol Lung Cell Mol Physiol*. 2006;291(4):L559-65. doi:10.1152/ajplung.00498.2005
10. Kim HY, Pang MF, Varner VD, et al. Localized Smooth Muscle Differentiation Is Essential for Epithelial Bifurcation during Branching Morphogenesis of the Mammalian Lung. *Dev Cell*. 2015;34(6):719-726. doi:10.1016/j.devcel.2015.08.012
11. Goodwin K, Mao S, Guyomar T, et al. Smooth muscle differentiation shapes domain branches during mouse lung development. *Development*. 2019;(October). doi:10.1242/dev.181172
12. Yin W, Kim H, Wang S, et al. The potassium channel KCNJ13 is essential for smooth muscle cytoskeletal organization during mouse tracheal tubulogenesis. *Nat Commun*. 2018:1-13. doi:10.1038/s41467-018-05043-5
13. Kishimoto K, Tamura M, Nishita M, et al. Synchronized mesenchymal cell polarization and differentiation shape the formation of the murine trachea and esophagus. *Nat Commun*. 2018;9(2816). doi:10.1038/s41467-018-05189-2
14. Zheng X-L. Myocardin and smooth muscle differentiation. *Arch Biochem Biophys*. 2014;543:48-56. doi:10.1016/j.abb.2013.12.015
15. Zhang W, Menke DB, Jiang M, et al. Spatial-temporal targeting of lung-specific

mesenchyme by a Tbx4 enhancer. *BMC Biol*. 2013;11:111. doi:10.1186/1741-7007-11-111

16. Huang J, Cheng L, Li J, et al. Myocardin regulates expression of contractile genes in smooth muscle cells and is required for closure of the ductus arteriosus in mice. *J Clin Invest*. 2008;118(2). doi:10.1172/JCI33304
17. Kim HY, Pang MF, Varner VD, et al. Localized Smooth Muscle Differentiation Is Essential for Epithelial Bifurcation during Branching Morphogenesis of the Mammalian Lung. *Dev Cell*. 2015;34(6):719-726. doi:10.1016/j.devcel.2015.08.012
18. Zhang WC, Peng YJ, Zhang GS, et al. Myosin light chain kinase is necessary for tonic airway smooth muscle contraction. *J Biol Chem*. 2010;285(8):5522-5531. doi:10.1074/jbc.M109.062836
19. Hines E a, Jones MN, Verheyden JM, Harvey JF, Sun X. Establishment of smooth muscle and cartilage juxtaposition in the developing mouse upper airways. *Proc Natl Acad Sci U S A*. 2013;110(48):19444-19449. doi:10.1073/pnas.1313223110/-/DCSupplemental.www.pnas.org/cgi/doi/10.1073/pnas.1313223110
20. Ovchinnikov DA, Deng JM, Ogunrinu G, Behringer RR. Col2a1-directed expression of Cre recombinase in differentiating chondrocytes in transgenic mice. *Genesis*. 2000;26(2):145-146. doi:10.1002/(SICI)1526-968X(200002)26:2<145::AID-GENE14>3.0.CO;2-C
21. Mandar Deepak Muzumdar, Bosiljka Tasic, Kazunari Miyamichi, Ling Li and LL. A Gobal Double-Flourescent Cre Reporter Mouse. *Genesis*. 2006;224(September):219-224. doi:10.1002/dvg

22. Yoshida CA, Yamamoto H, Fujita T, et al. Runx2 and Runx3 are essential for chondrocyte maturation , and Runx2 regulates limb growth through induction of Indian hedgehog. 2004:952-963. doi:10.1101/gad.1174704.and

23. Salingcarnboriboon R, Tsuji K, Komori T, Nakashima K, Ezura Y, Noda M. Runx2 Is a Target of Mechanical Unloading to Alter Osteoblastic Activity and Bone Formation in Vivo. 2006;147(5):2296-2305. doi:10.1210/en.2005-1020

24. Li X, Du X, Li D, et al. ITGBL1 Is a Runx2 Transcriptional Target and Promotes Breast Cancer Bone Metastasis by Activating the TGF b Signaling Pathway. 2015;75(16):3302-3314. doi:10.1158/0008-5472.CAN-15-0240

25. Felsenthal N, Zelzer E. Mechanical regulation of musculoskeletal system development. 2017;9:4271-4283. doi:10.1242/dev.151266

26. Watanabe H, Yamada Y. Mice lacking link protein develop dwarfism and craniofacial abnormalities. *Nat Genet*. 1999;21(2):225-229. doi:10.1038/6016

27. Song EK, Jeon J, Jang DG, et al. ITGBL1 modulates integrin activity to promote cartilage formation and protect against arthritis. 2018;7486(October):1-16.

28. Tadokoro T, Gao X, Hong CC, Hotten D, Hogan BLM. BMP signaling and cellular dynamics during regeneration of airway epithelium from basal progenitors. *Development*. 2016;143(5):764-773. doi:10.1242/dev.126656

29. Sparrow MP, Lamb JP. Ontogeny of airway smooth muscle: Structure, innervation, myogenesis and function in the fetal lung. *Respir Physiol Neurobiol*. 2003;137(2-3):361-372. doi:10.1016/S1569-9048(03)00159-9

30. Nelson CM, Gleghorn JP, Pang M, et al. Microfluidic chest cavities reveal that transmural pressure controls the rate of lung development. 2017:4328-4335.

doi:10.1242/dev.154823

31. Li J, Wang Z, Chu Q, Jiang K, Li J, Tang N. The Strength of Mechanical Forces Determines the Differentiation of Alveolar Epithelial Cells. *Dev Cell*. 2018;44(3):297-312.e5. doi:10.1016/j.devcel.2018.01.008
32. Buckley SMK, Waddington SN, Jezzard S, et al. Factors influencing adenovirus-mediated airway transduction in fetal mice. *Mol Ther*. 2005;12(3):484-492. doi:10.1016/j.ymthe.2005.02.020
33. Chen F, Marquez H, Kim YK, et al. Prenatal retinoid deficiency leads to airway hyperresponsiveness in adult mice. *J Clin Invest*. 2014;124(2):801-811. doi:10.1172/JCI70291
34. Lee JH, Tammela T, Hofree M, et al. Anatomically and Functionally Distinct Lung Mesenchymal Populations Marked by Lgr5 and Lgr6. *Cell*. 2017;170(6):1149-1163.e12. doi:10.1016/j.cell.2017.07.028
35. Zepp JA, Zacharias WJ, Frank DB, et al. Distinct Mesenchymal Lineages and Niches Promote Epithelial Self-Renewal and Myofibrogenesis in the Lung. *Cell*. 2017;170(6):1134-1148.e10. doi:10.1016/j.cell.2017.07.034
36. Volckaert T, Dill E, Campbell A, et al. Parabronchial smooth muscle constitutes an airway epithelial stem cell niche in the mouse lung after injury. *J Clin Invest*. 2011;121(11):4409-4419. doi:10.1172/JCI58097.)
37. Mailleux AA, Kelly R, Veltmaat JM, et al. Fgf10 expression identifies parabronchial smooth muscle cell progenitors and is required for their entry into the smooth muscle cell lineage. *Development*. 2005;132(9):2157-2166. doi:10.1242/dev.01795

38. Felsenthal N, Zelzer E. Mechanical regulation of musculoskeletal system development. *Development*. 2017;144(23):4271-4283. doi:10.1242/dev.151266

39. Rolfe RA, Nowlan NC, Kenny EM, et al. Identification of mechanosensitive genes during skeletal development: Alteration of genes associated with cytoskeletal rearrangement and cell signalling pathways. *BMC Genomics*. 2014;15(1). doi:10.1186/1471-2164-15-48

40. Du Y, Kitzmiller JA, Sridharan A, et al. Lung Gene Expression Analysis (LGEA): An integrative web portal for comprehensive gene expression data analysis in lung development. *Thorax*. 2017;72(5):481-484. doi:10.1136/thoraxjnl-2016-209598

41. Chung MI, Bujnis M, Barkauskas CE, Kobayashi Y, Hogan BLM. Niche-mediated BMP/SMAD signaling regulates lung alveolar stem cell proliferation and differentiation. *Dev*. 2018;145(9):1-10. doi:10.1242/dev.163014

42. Zepp JA, Zacharias WJ, Frank DB, et al. Distinct Mesenchymal Lineages and Niches Promote Epithelial Self-Renewal and Myofibrogenesis in the Lung. *Cell*. 2017;170(6):1134-1148.e10. doi:10.1016/j.cell.2017.07.034

43. Huang J, Min Lu M, Cheng L, et al. Myocardin is required for cardiomyocyte survival and maintenance of heart function. *Proc Natl Acad Sci U S A*. 2009;106(44):18734-18739. doi:10.1073/pnas.0910749106

44. He WQ, Peng YJ, Zhang WC, et al. Myosin Light Chain Kinase Is Central to Smooth Muscle Contraction and Required for Gastrointestinal Motility in Mice. *Gastroenterology*. 2008;135(2):610-620. doi:10.1053/j.gastro.2008.05.032

45. Abler LL, Mehta V, Keil KP, et al. A High Throughput in situ

Hybridization Method to Characterize mRNA Expression Patterns in the Fetal Mouse Lower Urogenital Tract. *J Vis Exp*. 2011;(54):2-7. doi:10.3791/2912

46. Dobin A, Davis CA, Schlesinger F, et al. STAR: Ultrafast universal RNA-seq aligner. *Bioinformatics*. 2013;29(1):15-21. doi:10.1093/bioinformatics/bts635
47. Liao Y, Smyth GK, Shi W. FeatureCounts: An efficient general purpose program for assigning sequence reads to genomic features. *Bioinformatics*. 2014;30(7):923-930. doi:10.1093/bioinformatics/btt656
48. Love MI, Huber W, Anders S. Moderated estimation of fold change and dispersion for RNA-seq data with DESeq2. *Genome Biol*. 2014;15(12):1-21. doi:10.1186/s13059-014-0550-8
49. Babicki S, Arndt D, Marcu A, et al. Heatmapper: web-enabled heat mapping for all. *Nucleic Acids Res*. 2016;44(W1):W147-W153. doi:10.1093/nar/gkw419

Figures

Young et al.
Figure 1

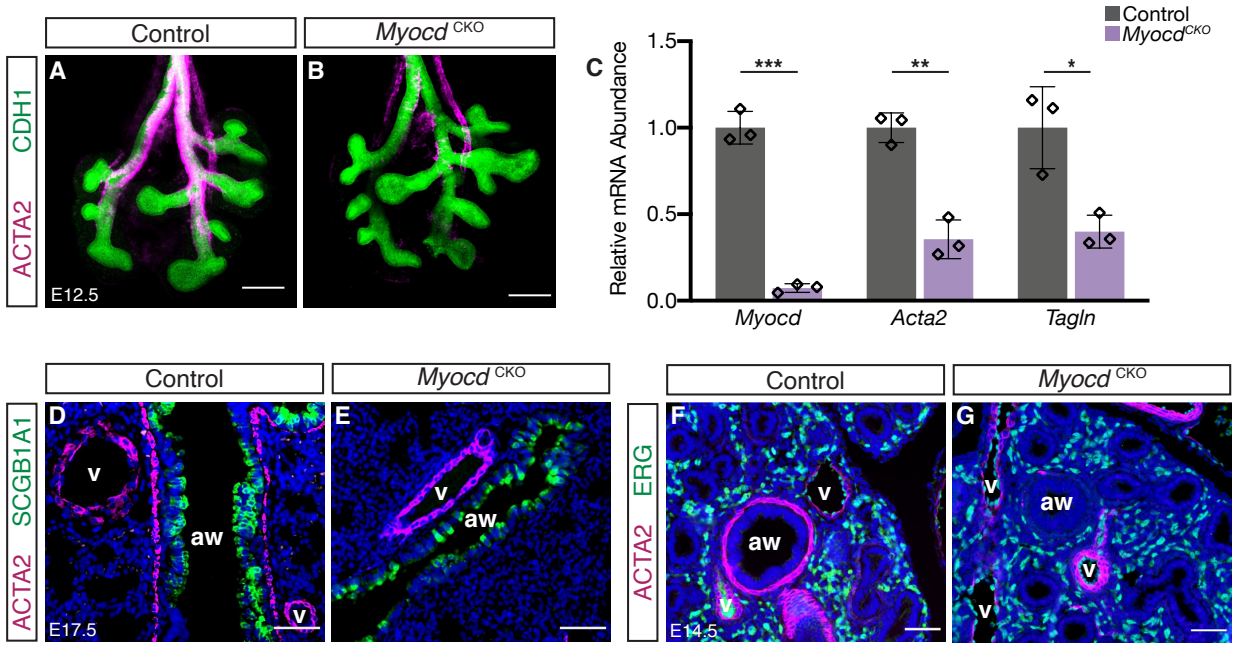

Figure 1. Airway smooth muscle differentiation is disrupted in *Myocd*^{CKO} lungs.

(A,B) Confocal images showing immunofluorescent detection of smooth muscle marker ACTA2 (magenta) and epithelium marker CDH1 (green) in whole lungs of control and *Myocd*^{CKO} mice at E12.5, showing near complete absence of airway smooth muscle adjacent to airways in *Myocd*^{CKO}. Scalebar: 200 μm. (C) qRT-PCR quantification of relative mRNA levels of *Myocd* and smooth muscle markers *Acta2* and *Tagln* in control and *Myocd*^{CKO} lungs at E12.5. Data are represented as individual points for each biological sample $\pm$ SD. *: $p<0.05$, **: $p<0.005$, ***: $p<0.0005$. (D-G) Immunofluorescent detection of ACTA2 (magenta), and club cell marker SCGB1A1 (green) (D,E) or endothelial marker ERG (green) (F,G) in lungs of control and *Myocd*^{CKO} at E17.5 and E14.5, showing the near absence of the airway (aw) smooth muscle and the persistence of vascular (v) smooth muscle in *Myocd*^{CKO}.

Young et al.
Figure 2

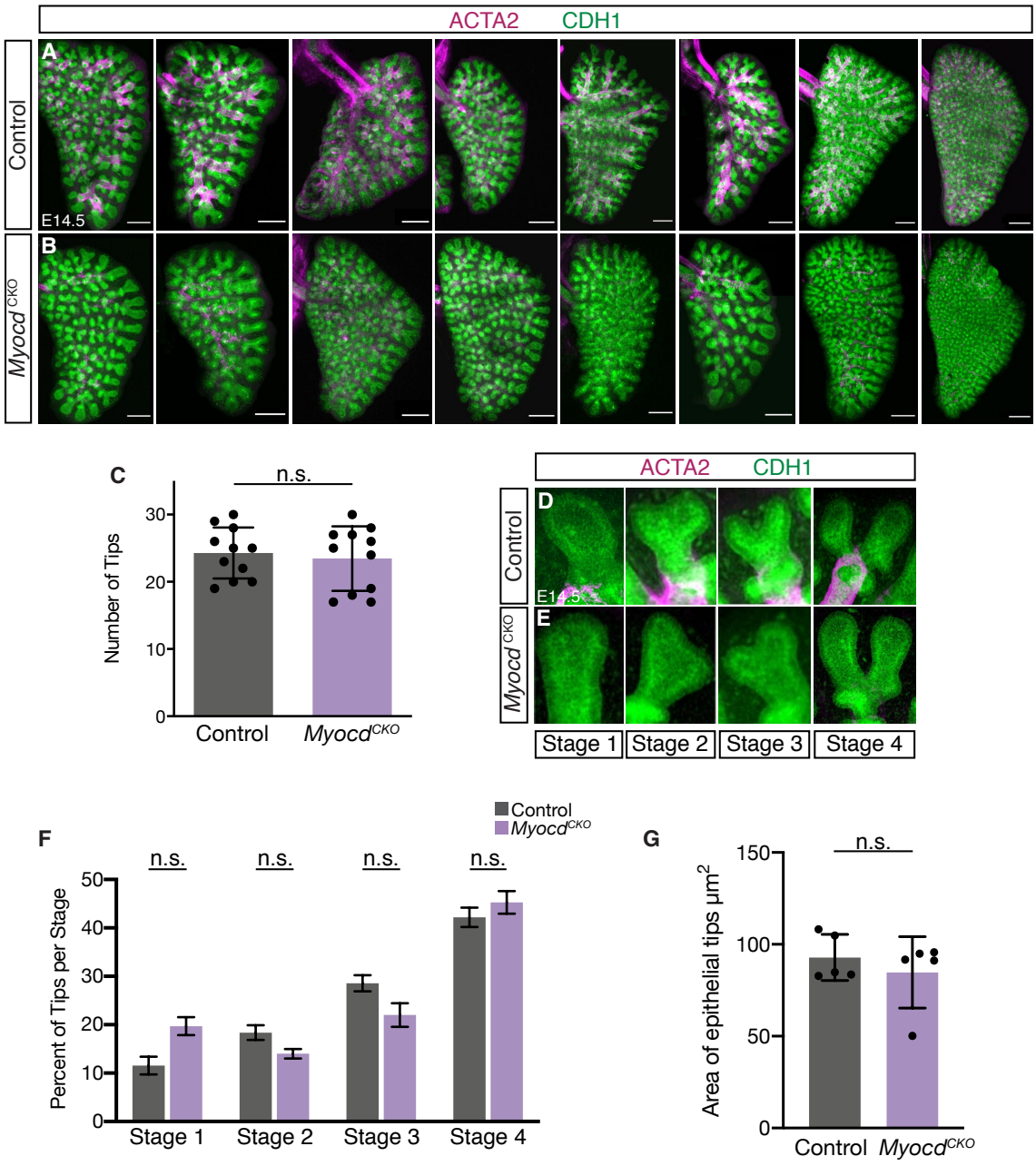

Figure 2. Loss of airway smooth muscle differentiation did not affect airway epithelial branching.

(A,B) Maximum projection of z-stacks from confocal images showing immunofluorescent detection of ACTA2 (magenta) and CDH1 (green) in left lung lobes of control and *Myocd*^{CKO} mice at E14.5, showing normal branching morphogenesis in *Myocd*^{CKO} lungs. Columns represent control and *Myocd*^{CKO} littermates. Scalebar: 250 μm. (C) Quantification of terminal epithelial tips in E14.5 control and *Myocd*^{CKO} left lung lobes, N=11 each. Data are represented as individual points for each biological sample ± SD. (D-E) Representative images showing immunofluorescent detection of ACTA2 (magenta) and CDH1 (green) in the four stages of epithelial tip bifurcation in control and *Myocd*^{CKO} lungs at E14.5. (F) Quantification of tips in each stage shown as a percentage of total tip number. Data are represented as individual points for each biological sample ± SD. (G) Quantification of epithelial tip areas shown as the average tip area per left lobe. Data are represented as mean ± SD.

Young et al.
Figure 3

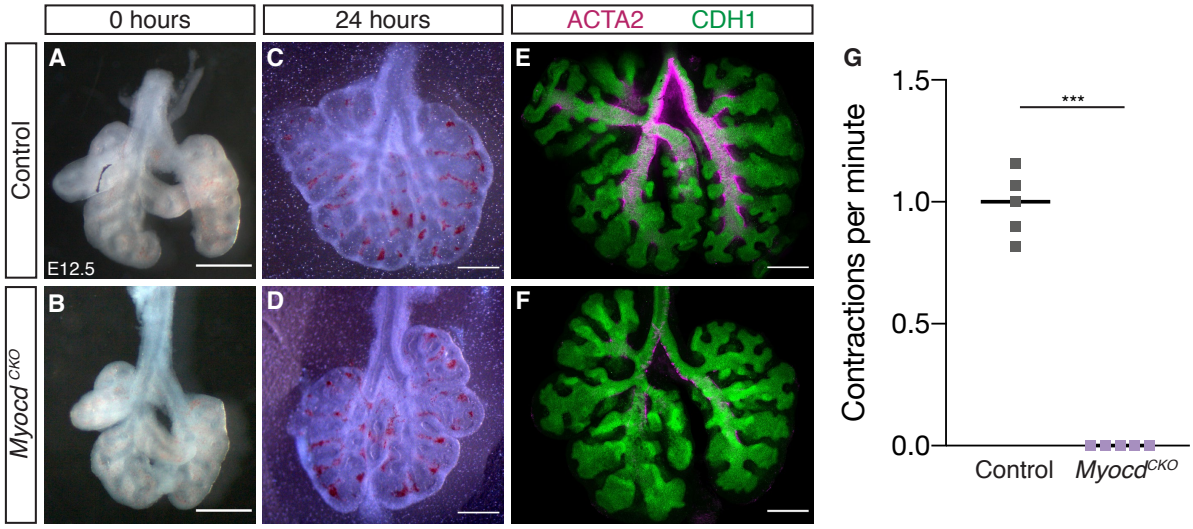

Figure 3. Loss of airway smooth muscle differentiation led to absence of airway peristalsis.

(A-B) Representative control and *Myocd*^{CKO} E12.5 lungs were dissected and imaged fresh, and (C,D) 24 hours after culture. Scalebar: 50 μm. (E,F) Representative maximum projection of z-stacks from confocal images showing immunofluorescent detection of ACTA2 (magenta) and CDH1 (green) in E12.5 cultured lungs, showing a lack of differentiated ASM in *Myocd*^{CKO} lung. Scalebar: 50 μm. (G) Peristalsis was observed in control airways approximately once a minute, while *Myocd*^{CKO} airways never contracted. Data are represented as individual points for each biological sample ± SD. ***: $p<0.0001$.

Young et al.
Figure 4

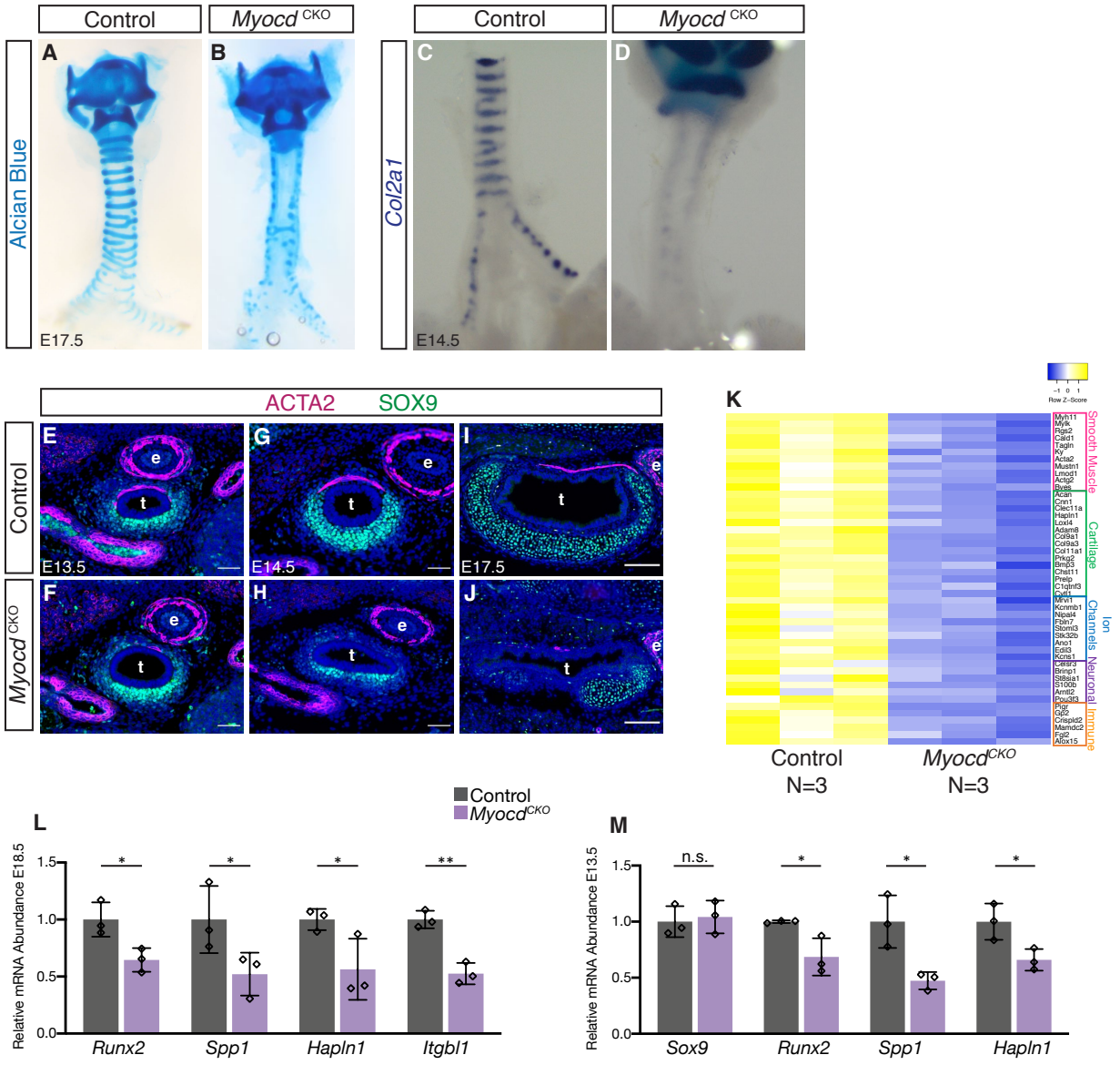

Figure 4. Loss of airway smooth muscle differentiation led to disrupted cartilage segmentation.

(A,B) Whole mount alcian blue staining showed cartilage segmentation defects in *Myocd*^{CKO} E18.5 tracheas. Scalebar: 50 μm. (C,D) *Col2a1* wholemount RNA in situ hybridization revealed reduced chondrocytes in *Myocd*^{CKO} E14.5 tracheas. Scalebar: 100 μm. (E-J) Immunofluorescent detection of ACTA2 (magenta) and cartilage marker SOX9 (green) expression in transverse sections of tracheas of control and *Myocd*^{CKO} at E13.5 (E,F), E14.5 (G,H), and E17.5 (I,J). Scalebar: 50 μm for E-H and 100 μm for I,J. "t" indicates trachea and "e" indicates esophagus. (K) Heatmap of RNA-seq data showing groups of significantly downregulated genes, by an adjusted p-value less than 0.05, in the *Myocd*^{CKO} E18.5 tracheas. (L) qRT-PCR quantification of relative mRNA levels of mechanosensitive genes *Runx2*, *Spp1, Hapln1*, and *Itgbl1* in control and *Myocd*^{CKO} tracheas at E18.5. *: $p<0.05$, **: $p<0.005$. (M) qRT-PCR quantification of relative mRNA levels of *Sox9* and mechanosensitive genes *Runx2*, *Spp1,* and *Hapln1* in control and *Myocd*^{CKO} tracheas at E13.5. *: $p<0.05$. Data are represented as individual points for each biological sample $\pm$ SD.

Young et al.
Figure 5

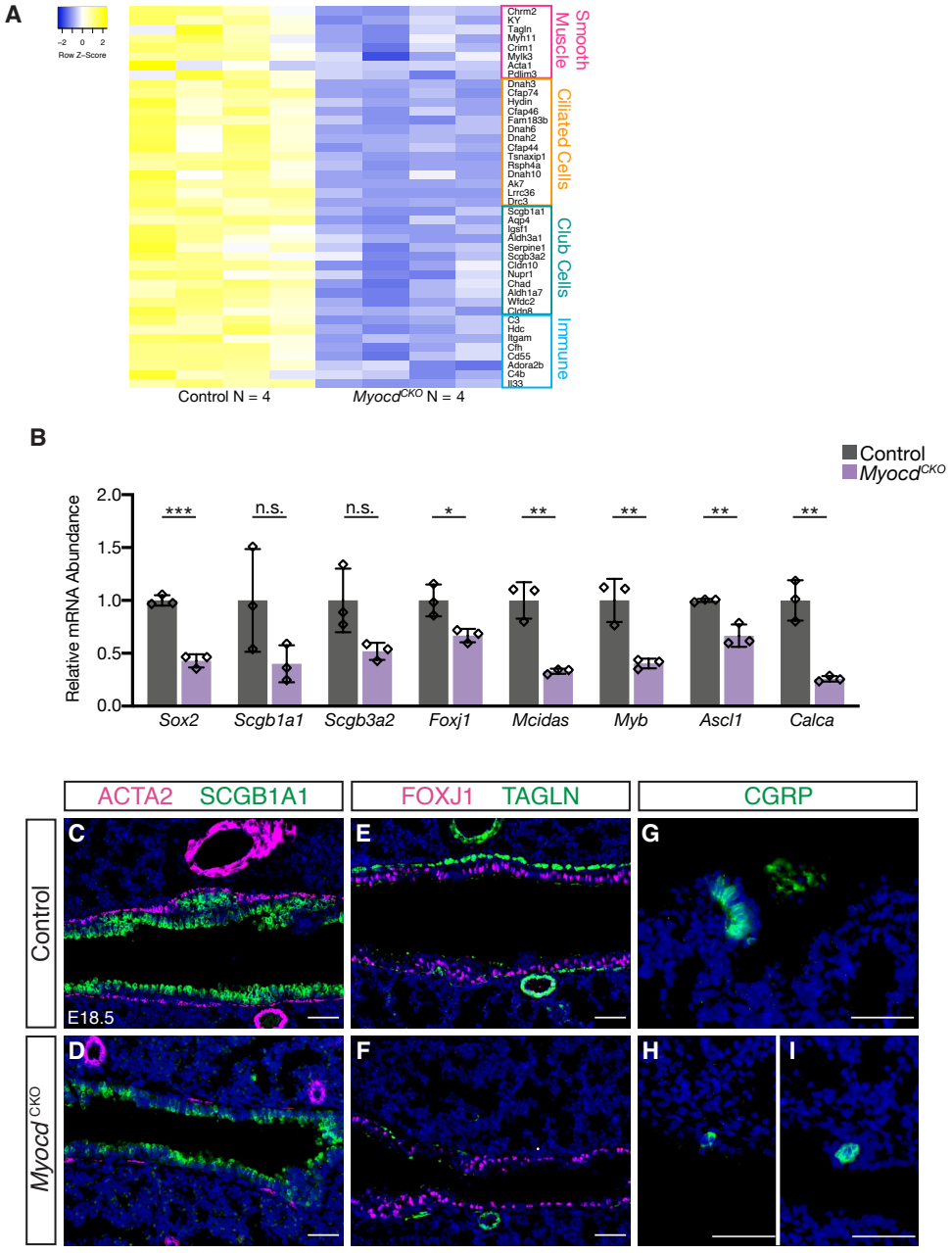

Figure 5. Loss of airway smooth muscle differentiation did not affect the ability of airway epithelial cells to differentiate.

(A) Heatmap of RNA-seq data showing selected groups of significantly downregulated genes, by an adjusted p-value less than 0.05, in the *Myocd*^{CKO} E18.5 lung. (B) qRT-PCR quantification of relative mRNA levels of airway epithelial cell marker genes for general airway epithelium *Sox2*; club cells *Scgb3a2* and *Scgb1a1*; ciliated cells *Foxj1, Mcidas* and *Myb*; pulmonary neuroendocrine cells *Ascl1* and *Calca*; in control and *Myocd*^{CKO} lungs at E18.5. Data are represented as individual points for each biological sample $\pm$ SD. *: $p<0.05$, **: $p<0.005$, ***: $p<0.0005$. (C,D) Immunofluorescent detection of ACTA2 (magenta) and SCGB1A1 (green). (E,F) Immunofluorescent detection of FOXJ1 (magenta) and smooth muscle marker TAGLN (green). (G-I) Immunofluorescent detection of CGRP (green) in control and *Myocd*^{CKO} E18.5 lungs. Scalebars: 50μm.

Young et al.
Figure 6

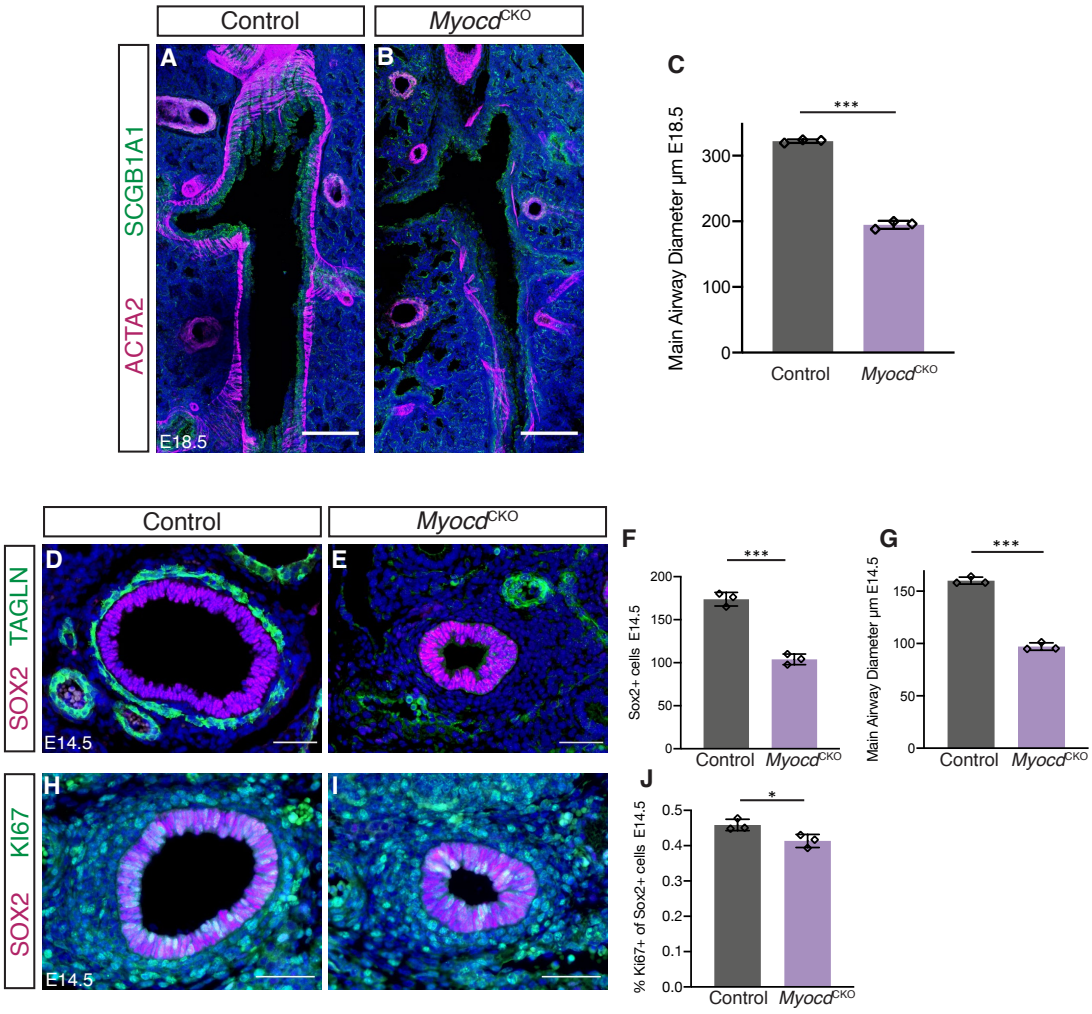

Figure 6. Loss of airway smooth muscle cell differentiation led to reduced airway size.

(A,B) Confocal stacks covering the entire thickness of the main airways in 100μm thick cryosections of E18.5 left lobes showing immunofluorescent detection of ACTA2 (magenta) and SCGB1A1 (green). Scalebar: 200 μm. (C) Quantification showing reduced main airway diameter in the mutant at E18.5.***: $p<0.0005$. (D,E) Immunofluorescent detection of airway epithelial marker SOX2 (magenta) and TAGLN (green) in transverse sections taken at equivalent depths of the main airway in control and *Myocd*^{CKO} lungs at E14.5. Scalebar: 50μm. (F) Quantification showing decreased number of SOX2^{+} cells in the *Myocd*^{CKO} main airway at E14.5. ***: $p<0.0005$. (G) Quantification showing decreased main airway diameter in the mutant at E14.5. ***: $p<0.0005$. (H,I) Immunofluorescent detection of SOX2 (magenta) and proliferation marker KI67 (green) in transverse sections taken at similar depths of the main airway in control and *Myocd*^{CKO} lungs at E14.5. Scalebar: 50μm. (J) Quantification showing decreased number of the percentage of Ki67^{+}SOX2^{+} proliferating cells in total Sox2^{+} airway epithelial cells in the *Myocd*^{CKO} main airway at E14.5. *: $p<0.05$. Data are represented as individual points for each biological sample $\pm$ SD.

Young et al.
Figure 7

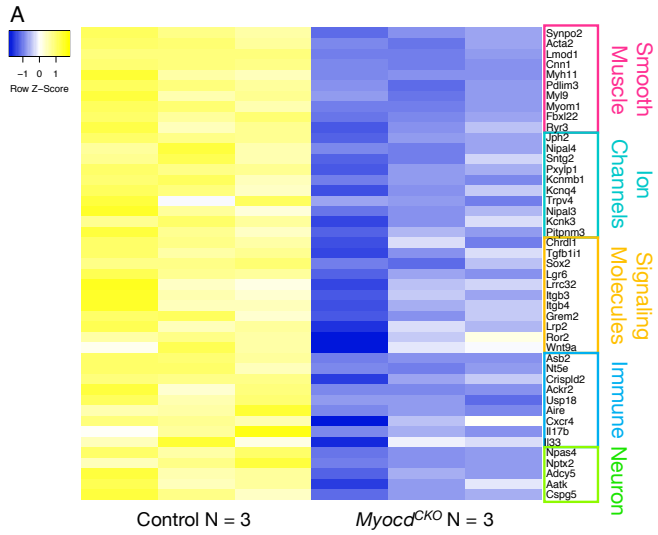

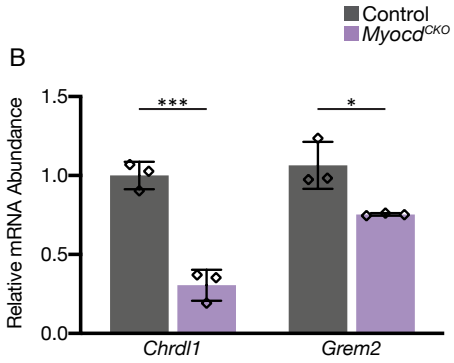

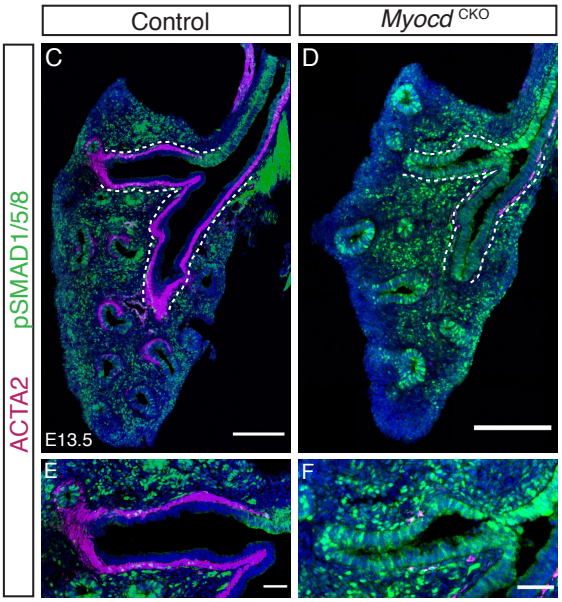

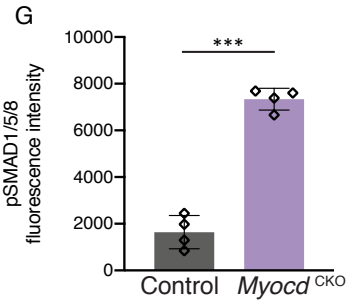

Figure 7. Loss of airway smooth muscle cell differentiation led to increased BMP activity in the main airway.

(A) Heatmap of RNA-seq data showing groups of significantly downregulated genes, by an adjusted p-value less than 0.05, in the *Myocd*^{CKO} E13.5 lung. (B) qRT-PCR quantification of relative mRNA levels of BMP4 antagonists *Chrdl1* and *Grem2* in control and *Myocd*^{CKO} lungs at E13.5. *: $p<0.05$, ***: $p<0.0005$. (C-F) Confocal images of 20 μm thick cryosections of the main pulmonary airway in E13.5 left lung showing immunofluorescent detection of ACTA2 (magenta) and BMP activity indicator pSMAD1/5/8 (green). Dashed lines represent the outline of the main pulmonary airway. Scalebar: 200 μm. (E,F) Magnified images of the first proximal branches region of C, D, respectively. (G) Quantification showing increased pSMAD1/5/8 signal in the main airways in *Myocd*^{CKO} compared to control. ***: $p<0.0005$. Data are represented as individual points for each biological sample $\pm$ SD.

Young et al.
Figure S1

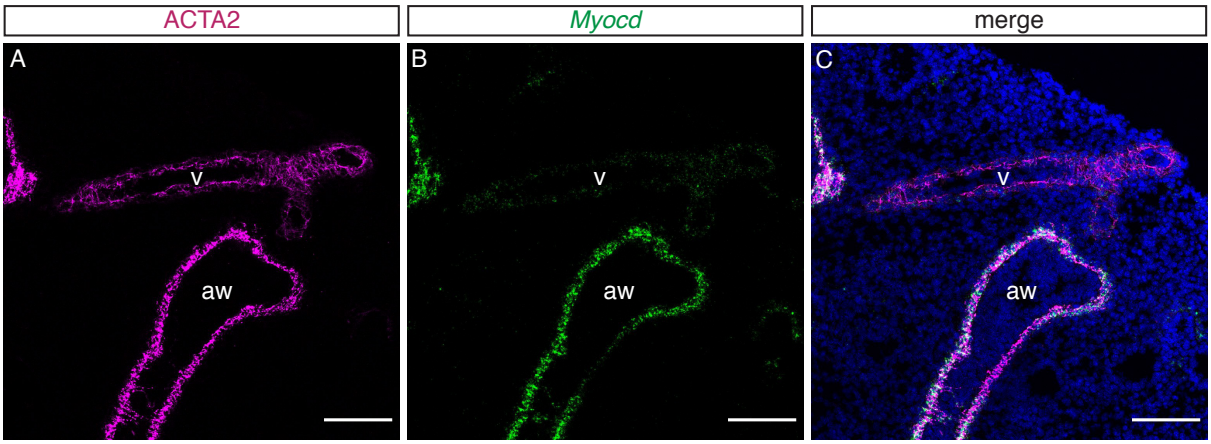

Supplemental Figure 1

(A-C) Representative immunofluorescent images of ACTA2 (magenta) (A) and RNAscope in situ detection of *Myocd* (green) (B) and merged with DAPI (C) of a E14.5 wild-type lung section. Scalebar: 100 μm.

Young et al.
Figure S2

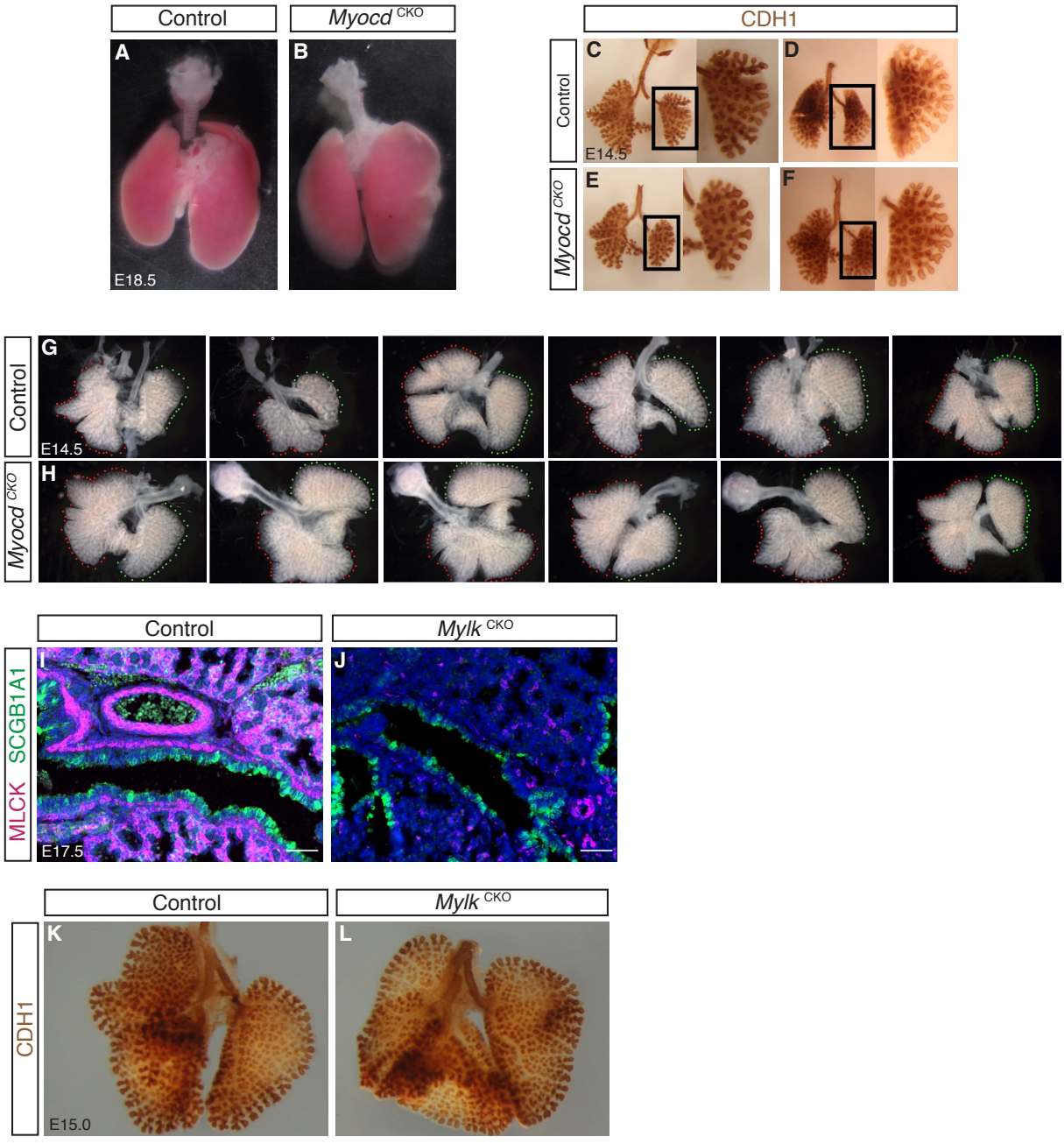

Supplemental Figure 2

(A,B) Brightfield images of whole lungs of control and *Myocd*^{CKO} at E18.5. (C-F) Immunohistochemistry detection of CDH1 in control and *Myocd*^{CKO} at E14.5. (G,H) Brightfield images of whole lungs of control and *Myocd*^{CKO} at E14.5 from mice in the C57Bl/6 genetic background. Green dots denote branched epithelial tips of left lobes, red dots denote branched epithelial tips of right lobes. (I,J) Immunofluorescent detection of MYLK (magenta) and SCGB1A1 (green) in lung sections in control and *Mylk*^{CKO} lungs at E17.5. Scalebar: 50 μm. (K,L) Immunohistochemistry detection of CDH1 in control and *Mylk*^{CKO} lungs at E15.0.

Young et al.
Figure S3

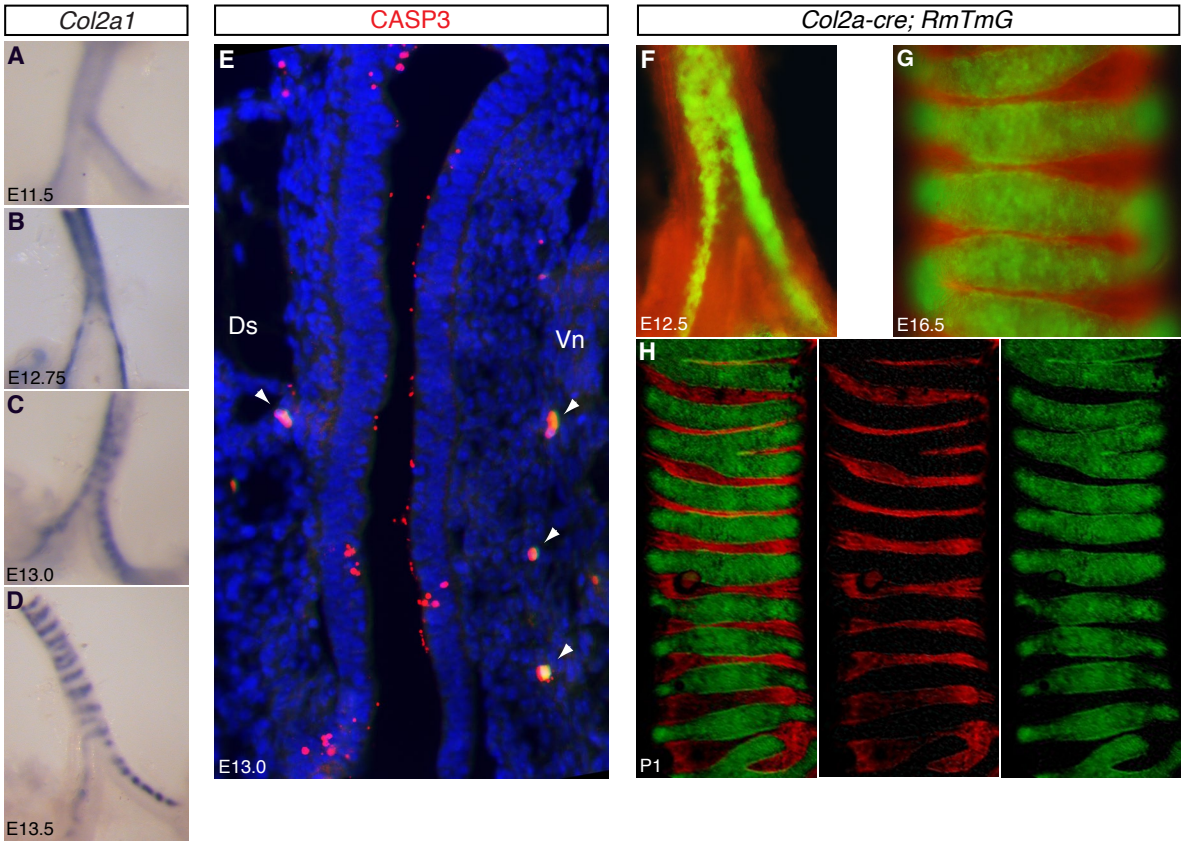

Supplemental Figure 3

(A-D) *Col2a1* RNA in situ of wild type tracheas at E11.5 (A), E12.75 (B), E13.0 (C), and E13.5 (D). (E) Immunofluorescent staining for apoptosis marker cleaved Caspase 3 (CASP3) (red) in an E13.0 longitudinal section of the trachea. Ds indicates the dorsal, smooth muscle side of the trachea and Vn indicates the ventral, cartilage side of the trachea. White arrowheads indicate red blood cells, identified by their auto-fluorescence in both the red and green channels. (F-H) *Col2a1-cre;RmTmG* tracheas at E12.5 (F), E16.5 (G) and postnatal day (P) 1 (H).

Young et al.
Figure S4

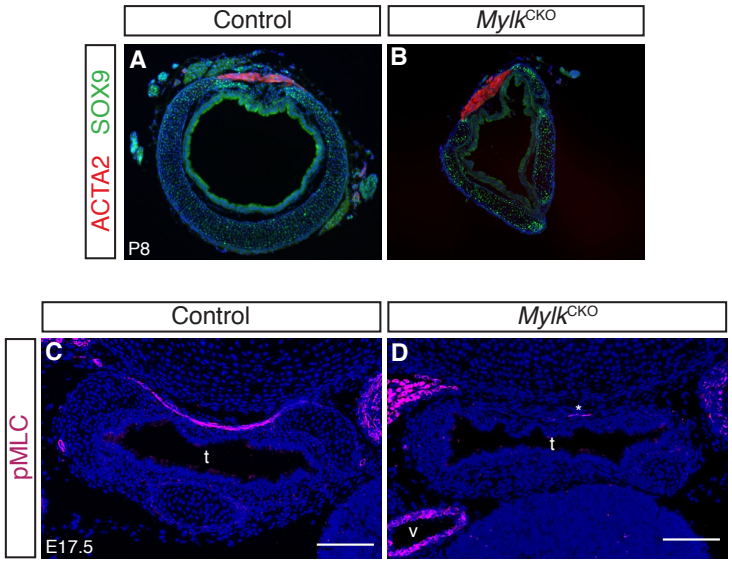

Supplemental Figure 4

(A,B) Immunofluorescent detection of ACTA2 (magenta) and SOX9 (green) in cross sections of tracheas at P8 of control and *Mylk*^{CKO} mice, showing disorganized cartilage in the *Mylk*^{CKO} trachea. (C,D) Immunofluorescent detection of phosphorylated myosin light chain (pMLC; magenta) in cross sections of tracheas at E17.5 of control and *Mylk*^{CKO} mice. Asterisk indicates drastically reduced pMLC signal in the *Mylk*^{CKO} trachea. t: trachea; v: vessel. Scalebar: 100 μm.

Young et al.
Figure S5

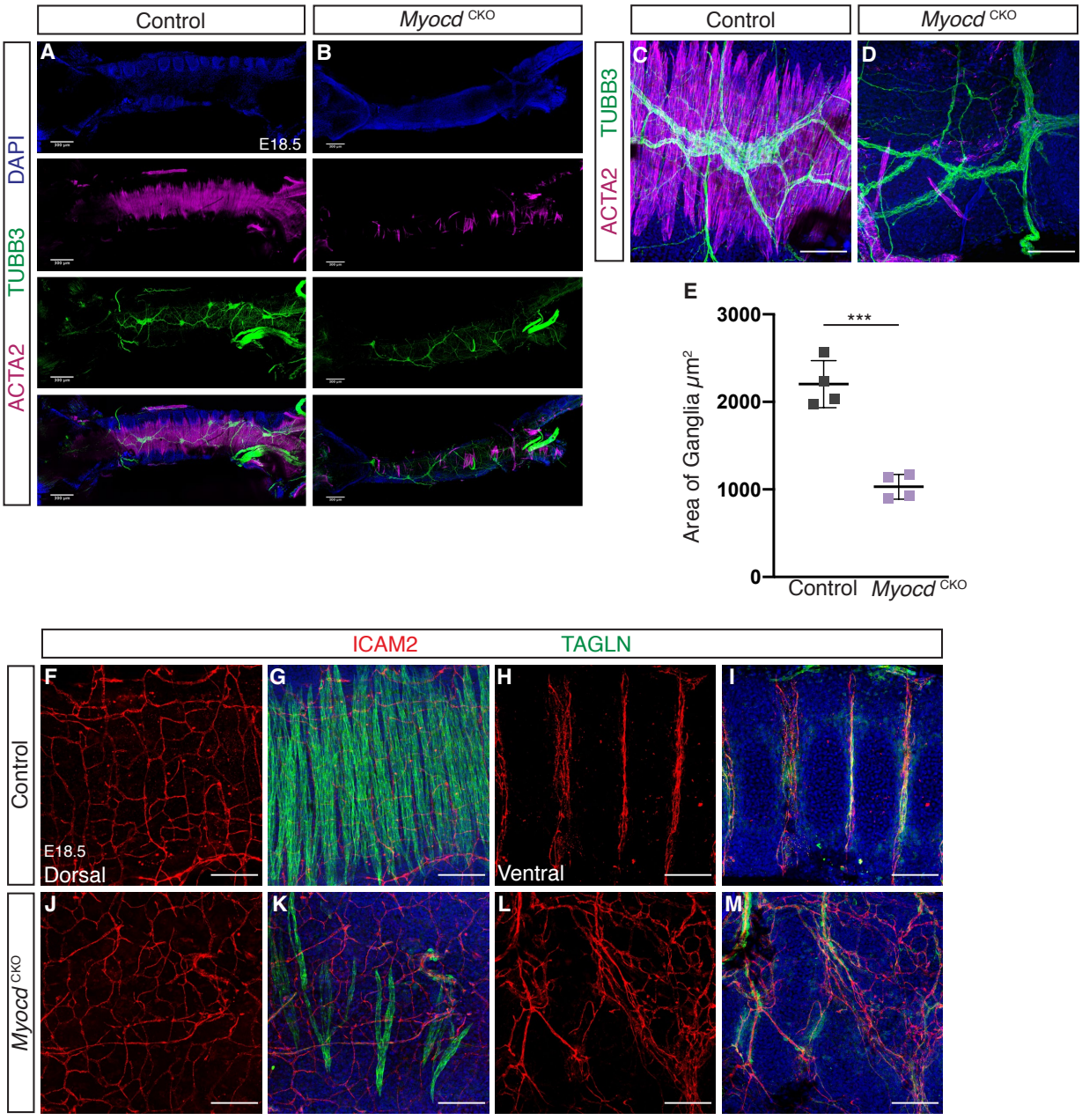

Supplemental Figure 5

(A-D) Confocal images showing immunofluorescent detection of ACTA2 (magenta) and nerve marker TUBB3 (also termed TUJ1) (green) in whole tracheas of control and *Myocd*^{CKO} mice at E18.5. (A,B) Scalebar: 300 μm. (C,D) Scalebar: 100 μm. (E) Quantification depicting the total area of ganglia in control and *Myocd*^{CKO} tracheas at E18.5, with each dot representing the cumulative ganglia area for an individual trachea. ***: $p<0.0005$. (F-M) Confocal images showing immunofluorescent detection of ICAM2 (red) and TAGLN (green) in whole tracheas of control and *Myocd*^{CKO} mice at E18.5. Dorsal side of trachea is shown in F,G,J,K; Ventral side of trachea is shown in H,I,L,M. Scalebar: 100 μm.

Young et al.
Figure S6

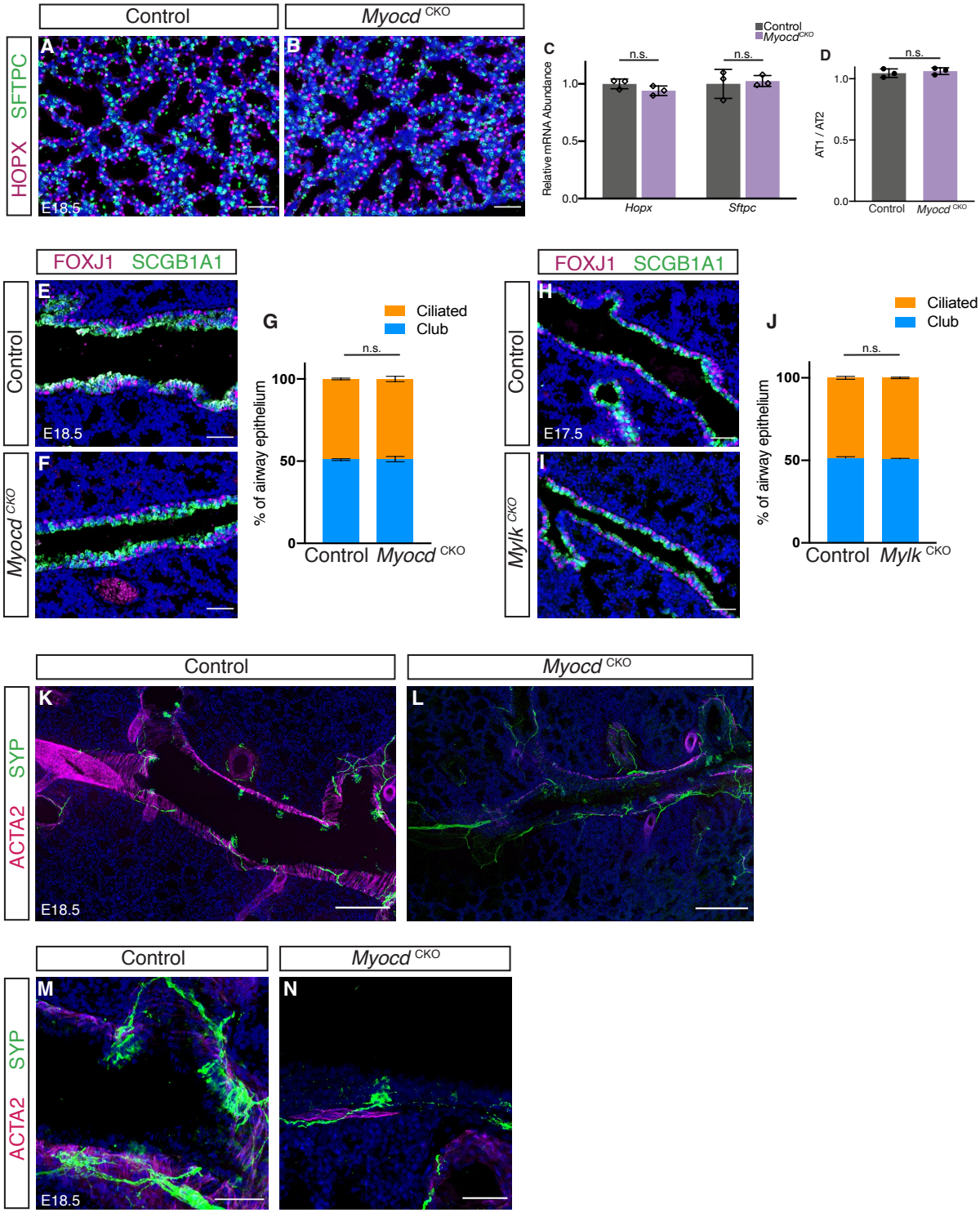

Supplemental Figure 6

(A,B) Immunofluorescent detection of alveolar type I marker HOPX (magenta) and alveolar type II marker SFTPC (green) in lung sections in control and *Myocd*^{CKO} lungs at E18.5. Scalebar: 50 μm. (C) qRT-PCR quantification of relative mRNA levels of *Hopx* and *Sftpc* in control and *Myocd*^{CKO} lungs at E18.5. (D) Quantification depicting the ratio of AT1 to AT2 cells in control and *Myocd*^{CKO} lungs at E18.5. (E,F) Immunofluroescent detection of FOXJ1 (magenta) and SCGB1A1 (green) in lung sections in control and *Mycod*^{CKO} lungs at E18.5. (G) Quantification depicting that club and ciliated cells each comprise approximately 50% of the airway epithelium in both the control and *Myocd*^{CKO} lungs at E18.5. (H,I) Immunofluroescent detection of FOXJ1 (magenta) and SCGB1A1 (green) in lung sections in control and *Mylk*^{CKO} lungs at E18.5. (J) Quantification depicting that club and ciliated cells each comprise approximately 50% of the airway epithelium in both the control and *Mylk*^{CKO} lungs at E18.5. (K-N) Confocal images showing immunofluorescent detection of ACTA2 (magenta) and SYP (green) in 70 μm thick cryo sections in control and *Myocd*^{CKO} main airways at E18.5. Scalebar: 200 μm (K,L), 50 μm (M,N). PNEC clusters are smaller in the mutant.

Young et al.
Figure S7

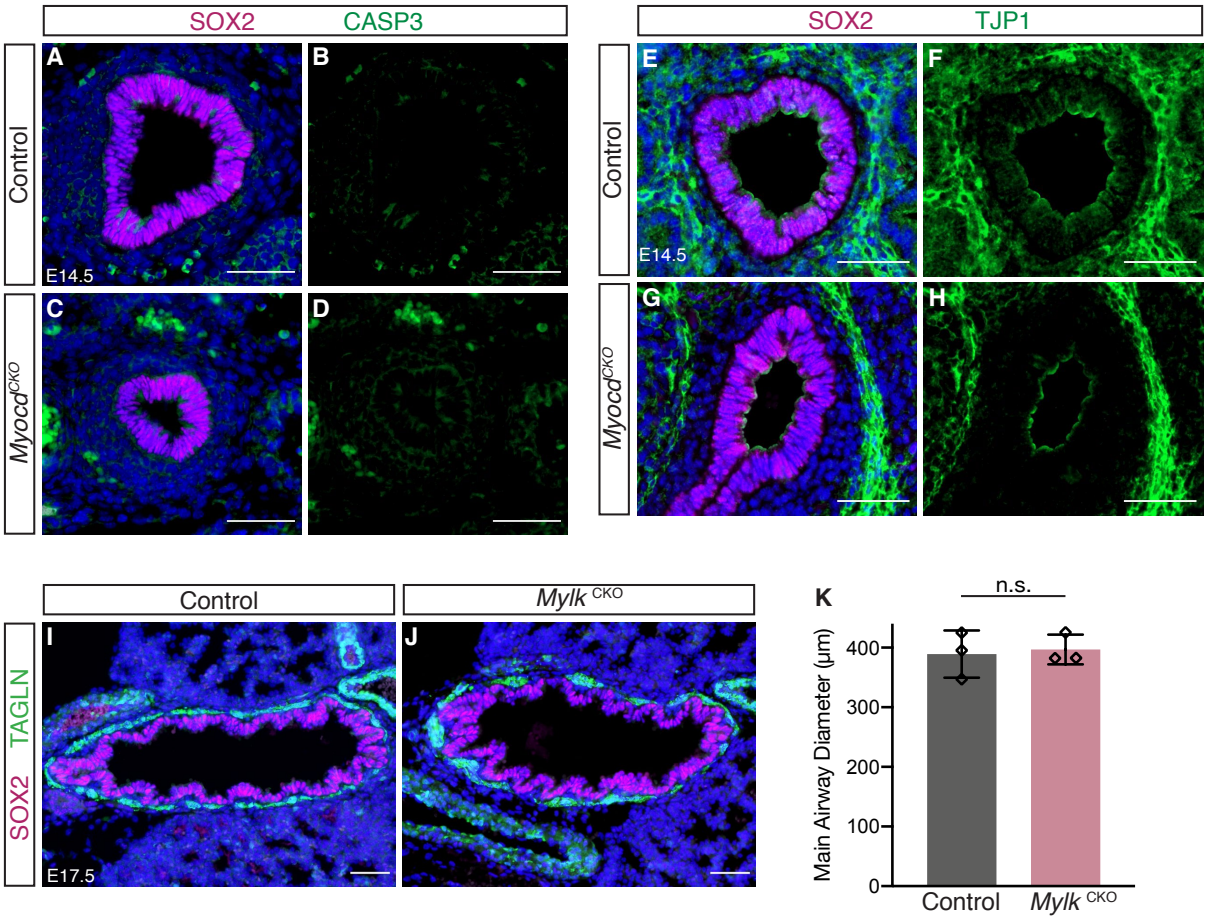

Supplemental Figure 7

(A-D) Immunofluorescent detection of SOX2 (magenta) and CASP3 (green) in transverse lung sections in control and *Myocd*^{CKO} main airways at E14.5, taken at similar depths. Scalebar: 50 μm. No signal was detected in the epithelium of either genotype. (E-H) Immunofluorescent detection of SOX2 (magenta) and tight junction marker TJP1 (also termed ZO-1; green) in transverse lung sections in control and *Myocd*^{CKO} main airways at E14.5. (I,J) Immunofluorescent detection of SOX2 (magenta) and TAGLN (green) in transverse lung sections in control and *Mylk*^{CKO} main airways at E17.5, taken at similar depths. Scalebar: 50 μm. (K) Quantification of airway diameter taken at similar depths in the control and *Mylk*^{CKO} main airways at E17.5, showing no difference in airway size.

Supplemental Movie Titles and Legends

Movie S1. Supplemental to Figure 3.

Peristalsis video for control lungs cultured for 24 hours. Video is a total of 6 seconds condensed from 10 minutes of filming.

Movie S2. Supplemental to Figure 3.

Peristalsis video for *Myocd*^{CKO} lungs cultured for 24 hours. Video is a total of 6 seconds long, condensed from 10 minutes of filming.

Chapter III: *E-cadherin* has a cell-type specific role in maintaining the integrity of pulmonary airways

Randee E. Young[1,3], Leah B. Nantie[3], Barsha Dash[1], Justinn Barr[1], Jamie M. Verheyden[1], Xin Sun[1,2,4]

[1]Department of Pediatrics, University of California-San Diego, La Jolla, CA 92093.

[2]Department of Biological Sciences, University of California-San Diego, La Jolla, CA 92093.

[3]Laboratory of Genetics, Department of Medical Genetics, University of Wisconsin-Madison, Madison, WI 53706.

[4]Lead contact

Corresponding Authors: Xin Sun (contact)
xinsun@ucsd.edu

Summary

E-cadherin is best known for its role in adherens junctions and establishing cell-cell contacts. However, it's function in airway homeostasis has not been thoroughly investigated. Recent evidence has shown that in allergic airway diseases *E-cadherin* is downregulated, although it is remains unclear whether decreased *E-cadherin* is a cause or consequence of airway remodeling. We set out to test the cell type specific role of *E-cadherin* by inactivating it's gene, *Cdh1*, in either pulmonary club cells or ciliated cells. We found that club cell, but not ciliated cell, *E-cadherin* is essential for maintaining airway epithelial proliferation and differentiation. In the absence of club cell *E-cadherin*, airways exhibit goblet cell metaplasia, mucus hypersecretion, and recruitment of immune cells. Our findings demonstrate the role of *E-cadherin* in maintaining airway homeostasis and provide insight to the molecular mechanisms underlying allergic airway inflammation.

Introduction

The pulmonary airways are in direct contact with the external environment and are constantly exposed to inhaled challenges including microbes, particulate matter, and allergens. The diverse cell types of the airway epithelium form a continuous barrier between the environment and the underlying tissue, and act as part of the innate immune system by serving as the first line of host defense. Intercellular junctions, including tight junctions which regulate the permeability of the barrier and adherens junctions which mechanically connect adjacent epithelial cells, form the structural adhesive forces of the airway. Adherens junctions initiate cell-cell contacts through E-cadherin (E-CAD). In addition to establishing adherens junctions, E-CAD plays a fundamental role in tissue morphogenesis by maintaining contact inhibition and regulating epithelial proliferation.

There is increasing evidence that disturbances of the airway epithelium may act as a driver for lung pathogenesis, particularly during allergic airway inflammation [1,2]. Environmental insults can break adherens junctions by displacing E-CAD, leading to infiltration of the airway epithelium, downstream immune reactions, and airway remodeling [3]. Lung biopsies from patients with allergic asthma display significant downregulation of E-CAD [4]. Additionally, animal models of induced allergen challenge exhibit a decreased E-CAD after allergen exposure [5]. However, it is unclear whether the observed downregulation in E-CAD occurs upstream or downstream of the immune changes that contribute to allergic airway inflammation.

Goblet cell metaplasia is a characteristic feature of lung diseases exhibiting allergic airway inflammation, including asthma and chronic obstructive pulmonary

disorder (COPD). Goblet cells are rarely observed in adult lungs during homeostasis. Mucus secretion generally serves to protect the airways from infection and injury, although excessive goblet cell differentiation and mucus hypersecretion contribute to airway disease pathogenesis. Many signaling factors control goblet cell differentiation, including the Notch and Wnt signaling pathways [6,7]. Immune factors, particularly type 2 cytokines, are known to play a prominent role in promoting goblet cell differentiation. IL4 and IL13 share many regulatory elements and signal through a shared functional receptor complex. They are critical effectors of type 2 immunity and key mediators of asthmatic phenotypes, notably including goblet cell metaplasia [8]. IL13 has been shown to regulate mucus production by directly stimulating airway epithelial cells to differentiate into goblet cells in vitro [7]. IL33 is an epithelial derived type 2 cytokine that can also induce goblet cell metaplasia in the lung, as well as the intestinal epithelium [9,10]. IL33 expression is regulated by *Spdef* and *Foxa3*, which are transcription factors necessary for goblet cell differentiation [11]. Goblet cell differentiation and mucus hypersecretion is multi-step process involving crosstalk between the airway epithelium and immune cells.

The underlying molecular mechanisms that control airway epithelial barrier function and their role in disease pathogenesis are not fully understood. Given the role of E-CAD in not only maintaining adherens junctions, but also acting as a critical regulator of epithelial cellular behavior, we set out to test the role of E-CAD in maintaining lung homeostasis. We found that E-CAD is required for airway epithelial cell maintenance, and the loss of E-CAD leads to downstream immune response, airway

remodeling, and goblet cell metaplasia. Surprisingly, we found that E-CAD regulates airway homeostasis in a cell type specific manner.

Results

Cdh1 inactivation in pulmonary club cells causes cellular proliferation, altered differentiation, and severe goblet cell metaplasia

Club and ciliated cells are the two major cell types of the airway epithelium and together represent more than 90% of airway epithelial cells. To determine the role of E-CAD in maintaining lung homeostasis in each of these cell types, we conditionally inactivated it's gene, *Cdh1,* by generating *Scgb1a1-creER^{TM}; Cdh1$^{flox/flox}$* mice; hereafter referred to as *Scgb1a1^{creERT}; Cdh1^{CKO}* , and *Foxj1-creERT2; Cdh1$^{flox/flox}$* mice; hereafter referred to as *Foxj1^{creERT2}; Cdh1^{CKO}* [12–14]. To observe the effect of E-CAD in maintaining homeostasis, adult *Scgb1a1^{creERT}; Cdh1^{CKO}* and *Foxj1^{creERT2}; Cdh1^{CKO}* mice were given four injections of tamoxifen for four consecutive days, and their lungs were harvested two weeks after the final injection (Figure 1A).

In the club cell mutant, loss of *Cdh1* led to airway thickening (Figure 1B). Crossing the *Scgb1a1^{creERT}; Cdh1^{CKO}* mice to the nuclear *Cre* reporter *Rosa^{Sun1GFP}* allowed us to observe the lineage of the *Scgb1a1^{creERT}; Cdh1^{CKO}; Rosa^{Sun1GFP}* cells [15]. To investigate the cellular origins of the thickened airways, we examined proliferation by KI67 immunostaining in *Scgb1a1^{creERT}; Cdh1^{CKO}; Rosa^{Sun1GFP}* lungs and find that cellular proliferation was significantly increased in the airway epithelium and proliferating cells are from the *Scgb1a1^{creERT}; Cdh1^{CKO}; Rosa^{Sun1GFP}* club cells (Figure 1C,D). While the proliferating cells in the airway are all SOX2+ epithelial cells, they are not positive for the ciliated cell marker FOXJ1 confirming that ciliated cells are not the source of increased cellular proliferation (Supplemental Figure 1A).

We next quantified cell population changes in the *Scgb1a1^{creERT}; Cdh1^{CKO}; Rosa^{Sun1GFP}* lungs by fluorescence-activated cell sorting (FACS). Compared to controls (*Scgb1a1^{creERT}; Cdh1$^{fl/+}$; Rosa^{Sun1GFP}*), *Scgb1a1^{creERT}; Cdh1^{CKO}; Rosa^{Sun1GFP}* lungs have a slightly higher proportion of total epithelial cells, and a significantly higher number of lineage labelled GFP+ epithelial cells following inactivation of *Cdh1* (Supplemental Figure 1B,C). These findings were substantiated by manual cell counting which revealed that in control airways, *Scgb1a1^{creERT}; Cdh1$^{fl/+}$; Rosa^{Sun1GFP}* lineage cells represent ~60% of the airway epithelial cells (SOX2+) compared to an increase to ~80% in the *Scgb1a1^{creERT}; Cdh1^{CKO}; Rosa^{Sun1GFP}* lungs (Figure 1E,F). These data together suggest that inactivation of *Cdh1* in club cells led to over proliferation of these cells and overrepresentation of mutant cells in the airway epithelium, which likely contributed to the airway thickening phenotype.

We further investigated airway epithelial cell composition, and found that ciliated cells are significantly increased in the lungs of *Scgb1a1^{creERT}; Cdh1^{CKO}* mice (Figure 1G,H). Crossing the *Scgb1a1^{creERT}; Cdh1^{CKO}* mice to the cellular *Cre* reporter *Rosa^{TdTom}*, we observed the increase in ciliated cells originate from *Scgb1a1^{creERT}; Cdh1^{CKO}; Rosa^{TdTom}* lineage club cells (Figure 1I,J) [16].

Club cells are also known to differentiate into goblet cells during pathological conditions, we therefore tested whether goblet cells were affected in the *Scgb1a1^{creERT}; Cdh1^{CKO}* airways. While goblet cells are rarely detected in the airway epithelium of control mice, we observed a dramatic increase in goblet cells in the *Scgb1a1^{creERT}; Cdh1^{CKO}* airway epithelium (Figure 1K,L). In addition to increased immunostaining and expression of MUC5AC and AGR2 goblet cell markers, we also observed increased

expression of *Spdef* and *Foxa3* which are key transcription factors that control club to goblet cell differentiation (Figure 1L). This suggests that in addition to mucus overproduction, there is also precocious differentiation of goblet cells leading to significant goblet cell metaplasia in the *Scgb1a1*^{creERT}*; Cdh1*^{CKO} airways. Utilizing the *Scgb1a1*^{creERT}*; Cdh1*^{CKO}*; Rosa*^{TdTom} mice, we observed that goblet cells in the mutant airways originate from lineage labelled club cells that have lost *Cdh1* (Figure 1M).

In line with the increased conversion of club cells to ciliated and goblet cells, there is a significant decrease of club cells by staining and gene expression, despite increased proliferation of these cells (Figure 1G,H).

Cdh1 inactivation in ciliated cells does not cause airway remodeling

Inactivation of *Cdh1* in ciliated cells in *Foxj1*^{creERT2}*; Cdh1*^{CKO} mice led to a different phenotype compared to the club cell mutant. This is despite the same inactivation timing and a similar level of *Cdh1* downregulation in the two mutants (Figure 1F, Figure 2F).

Unlike the club cell *Cdh1* mutant, the *Foxj1*^{creERT2}*; Cdh1*^{CKO} lungs do not exhibit airway epithelial thickening, increased cellular proliferation, or aberrant airway epithelial differentiation (Figure 2A-D). Utilizing *Foxj1*^{creERT2}*; Cdh1*^{CKO}*; Rosa*^{Sun1GFP} mice, we analyzed the lineage of the *Cdh1* mutant ciliated cells. Compared to the controls, the *Foxj1*^{creERT2}*; Cdh1*^{CKO}*; Rosa*^{Sun1GFP} airways do not exhibit an increase of *Foxj1*^{creERT2}*; Cdh1*^{CKO} lineage cells (Figure 2E,F).

Interestingly, we did observe mild goblet cell metaplasia in *Foxj1*^{creERT2}*; Cdh1*^{CKO} mutant lungs resulting in an increase of MUC5AC+ cells and goblet cell gene

expression (Figure 2G,H). Compared to the dramatic increase of goblet cell marker expression in *Scgb1a1^{creERT}; Cdh1^{CKO}* mutant, these markers, such as X, are not as up-regulated in the *Foxj1^{creERT2}; Cdh1^{CKO}* lung. We observe a drastic difference in airway response to the loss of *E-cadherin* in club cells vs ciliated cells.

Cytokines are upregulated and immune cells are recruited to airways following loss of club cell *Cdh1*

Strong lines of evidence have demonstrated that goblet cell metaplasia and hypersecretion can be induced by increased type 2 cytokines including IL4 and IL13 [8]. Upstream of IL4 and IL13 is IL33, an epithelial derived cytokine that has been linked to goblet cell metaplasia in the lung and intestinal epithelium [9,10]. To determine if goblet cell metaplasia could be due to a change in immune signature in the *Scgb1a1^{creERT}; Cdh1^{CKO}* airway, we analyzed the expression of type 2 cytokines by qRT-PCR. We observe a significant increase in *Il33*, *Il4*, and *Il13* expression in the *Scgb1a1^{creERT}; Cdh1^{CKO}* lungs, but not *Il5* (Figure 3A). Consistent with their roles in type 2 immunity, we observed an increase of CD45+ cells adjacent to the airways in the *Scgb1a1^{creERT}; Cdh1^{CKO}* mutant lung compared to control (Figure 3B). Similar to the pattern of goblet cell metaplasia, airway inflammation is present throughout the proximal to distal main airway (Figure 3B). Intriguingly, *Foxj1^{creERT2}; Cdh1^{CKO}* lungs revealed no increase of type 2 cytokine expression or immune cell infiltration by CD45 staining (Figure 3C,D). These findings suggest there are distinct mechanisms that underlie the goblet cell metaplasia phenotypes observed in club vs ciliated cell *Cdh1* mutants.

To further dissect the inflammatory changes in the *Scgb1a1^{creERT}; Cdh1^{CKO}* mutant, we determined the composition of the increased immune cells in the mutant. T cells are core effectors of Th2 immune response, and a key source of IL4 and IL13 during response to allergen challenge in mice [17]. In *Scgb1a1^{creERT}; Cdh1^{CKO}* lungs, we observed a notable increase of CD3+ T cells clustered near the airways (Figure 3E). There is also an increase of B cells, although less prominent than the increase in T cells (Supplemental Figure 2A). The co-presences of T and B cells under the airway is reminiscent of inducible bronchus associated lymphoid tissue (iBALT) described in lungs with high levels of inflammation or infection (Supplemental Figure 2B) [18]. In addition to immune cell increases, we also observe an increase in cellular proliferation in the sub-epithelial layer, but not in the airway smooth muscle (Supplemental Figure 2C).

To systematically explore gene expression changes that may underlie the cellular phenotypes, we first performed bulk RNA-seq on control and *Scgb1a1^{creERT}; Cdh1^{CKO}* whole lungs. Of the 1,537 significantly upregulated genes and 573 significantly downregulated genes (adjusted $p < 0.05$) pathway analysis revealed changes in epithelial cell differentiation, ciliated cell differentiation, and immune signaling (Supplemental Figure 2D). Among upregulated cytokines and immune regulators are the pro-inflammatory cytokines *Il6* and *Cxcl15* (also known as *Il8*) which are known to play a role in asthma pathogenesis, and immune cell recruitment genes including *Clu*, *Ccl20*, *Cxcl5, Cxcl13*, *Cxcl17* (Figure 3F,G). As expected, we observe that many genes associated with pulmonary club cells are significantly downregulated, while goblet and ciliated cell related genes are upregulated (Figure 3F,G). Interestingly, epithelial tight

junction Claudin genes are upregulated suggesting there may be compensation of tight junctions in the absence of *E-cadherin* dependent adherens junctions (Figure 3F,G).

The most significantly downregulated and differentially expressed gene was *Pon1* (Figure 3F,G). *Pon1* is an antioxidant enzyme synthesized by the liver where it is secreted into circulation and binds high-density lipoproteins [19]. PON1 may also play a protective role in the liver by protecting against inflammation and oxidative stress. In the context of the lung, PON1 has been implicated in inflammatory airway diseases including asthma and COPD, and overexpression of *Pon1* was correlated with reduced cytokine activity following mouse allergen challenge [20–26]. However, PON1 has not been thoroughly investigated in the lung, and it's role in the airway epithelium is unknown. We found that PON1 immunostaining significantly overlaps with SCGB1A1 in control airways, suggesting PON1 may be a marker of club cells (Figure 3H). Surprisingly, we found that PON1 immunostaining and expression by qRT-PCR is significantly reduced in the *Scgb1a1*^{creERT}*; Cdh1*^{CKO} lung (Figure 3H,I).

Goblet cell metaplasia is partially dependent on type 2 immune signaling

At the center of the observed cytokine expression changes are IL4 and IL13, core effectors of type 2 responses including goblet cell metaplasia and immune cell recruitment [8]. IL4 and IL13 signal through a shared functional receptor complex that consists of the type II receptor IL4R and its subunits: IL4Rα and IL13Rα1. IL4Rα is required for mediating the effects of IL4 and IL13 following OVA challenge [27,28]. To address if these phenotypes observed in the club cell mutants were dependent on increased IL4 and IL13 signaling, we introduced a null allele of IL4Rα in club cell mutant

background generating *Scgb1a1^{creERT}; Cdh1^{CKO}; Il4Rα^{KO}* mice [29]. Based on AGR2 immunostaining and *Muc5ac* qRT-PCR analysis, *Scgb1a1^{creERT}; Cdh1^{CKO}; Il4Rα^{KO}* mice exhibit an intermediate goblet cell phenotype, lower compared to *Scgb1a1^{creERT}; Cdh1^{CKO}; Il4Rα$^{+/-}$* lungs, and higher when compared to controls (Figure 4A,B). We observe no phenotypic difference between the *Scgb1a1^{creERT}; Cdh1^{CKO}; Il4Rα$^{+/-}$* heterozygous nulls and the *Scgb1a1^{creERT}; Cdh1^{CKO}* mice. These results suggest a partial rescue of goblet cell metaplasia in *Scgb1a1^{creERT}; Cdh1^{CKO}; Il4Rα^{KO}* double mutants. Based on CD45 staining and qRT-PCR analysis of type 2 cytokine expression, there was no significant difference in immune cell recruitment phenotype in the *Scgb1a1^{creERT}; Cdh1^{CKO}; Il4Rα^{KO}* lungs compared to *Scgb1a1^{creERT}; Cdh1^{CKO}* lungs, suggesting that immune cell recruitment occurs upstream or independent of *Il4Rα* signaling (Figure 4A,C).

Interestingly, the *Scgb1a1^{creERT}; Cdh1^{CKO}; Il4Rα^{KO}* double mutants displayed an increase of airway epithelial proliferation and differentiation of ciliated cells similar to that of the *Scgb1a1^{creERT}; Cdh1^{CKO}* mice by FOXJ1 staining and gene expression (Figure 4D,G). Similar to the goblet cell phenotype, we observed a partial rescue of club cells by SCGB1A1 and PON1 immunostaining and qRT-PCR analysis (Figure 4D, F,G). These findings suggest that the increased airway epithelial proliferation and increased differentiation of ciliated cells occur independently of *Il4Rα* mediated type 2 immune signaling.

The partial rescue of goblet cell metaplasia in the *Scgb1a1^{creERT}; Cdh1^{CKO}; Il4Rα^{KO}* airways suggest there are multiple pathways to achieving goblet cell differentiation, including type 2 immune independent mechanisms. To determine if club

cells autonomously differentiate into goblet cells upon loss of *Cdh1*, we generated mosaic *Scgb1a1*^{creERT}*; Cdh1*^{CKO} mice by injecting a single low dose of Tamoxifen. This low level of Tamoxifen induced recombination in a subset of club cells, allowing us to distinguish goblet cells arising from *Cdh1* mutant and control cells. We found that both lineage traced and non-recombined cells express AGR2 by immunostaining (Supplemental Figure 3A). Similarly, PON1 immunostaining revealed lineage traced and non-recombined cells downregulate PON1 following mosaic inactivation of E-CAD (Supplemental Figure 3A). This suggests that the following loss of *Cdh1,* club cells can differentiate into goblet cells autonomously and non-autonomously.

Discussion

The airway epithelium is a prominent site of pathogenesis in many lung diseases, including asthma. The inability of the airway epithelium to maintain a functional barrier has been hypothesized as a potential disease mechanism. An emerging phenotype of asthma is the downregulation of E-CAD in the airway epithelium [4,5]. In vitro studies have shown that loss of CDH1 in cultured human bronchial epithelial cells leads to increased production of inflammatory signals and Th2 cytokines [30]. Additionally, CDH1 polymorphisms in asthmatic patients are associated with airway remodeling and lung function [31]. Many allergens, including the common house dust mite (HDM), are known to cause epithelial damage by disrupting E-CAD meditated cell-cell adhesion leading to a loss of barrier integrity [32,33]. It is unknown whether the loss of E-CAD in asthmatic airways is a consequence or cause of this common disease.

Here, we find in the absence of allergen challenges or other introduced harms, the inactivation of *Cdh1* specifically in pulmonary club cells leads to significant airway remodeling, including goblet cell metaplasia and immune cell recruitment to the airways. These observed airway remodeling changes have similar characteristics of asthma phenotypes. Our study supports the hypothesis that the loss of E-CAD may cause asthma-like symptoms and can directly contribute to airway pathogenesis.

The most prominent role of E-CAD is maintaining adherens junctions and the integrity of epithelial barrier tissues. In addition to mechanically connecting epithelial cells, E-CAD is a critical regulator of cellular proliferation by acting as a sensor of cellular density and maintaining contact inhibition [34]. Loss of *Cdh1* in the developing lung epithelium results in alveolar simplification, airway denuding, and increased goblet

and immune cells [35]. *Cdh1* deletion in the adult lung epithelium impairs airway epithelial regeneration following naphthalene injury [36]. However, these studies inactivate *Cdh1* in both the airway and alveolar epithelium, as well as during developmental stages, making the role of E-CAD in airway epithelial maintenance unclear. Nonetheless, these previous studies suggest a role for E-CAD during lung development, epithelial differentiation, and maintenance.

Given the diversity of epithelial cells in the lung, we sought out to determine the cell-type specific role of *Cdh1* in maintaining adult airway homeostasis. We observed that following inactivation of *Cdh1* in *Scgb1a1*^{creERT}*; Cdh1*^{CKO} mice, mutant cells become overrepresented in the airway epithelium and exhibit distinctive behaviors including 1) increased proliferation, 2) increased differentiation into ciliated cells, and 3) metaplasia into goblet cells (Figure 5). This increased proliferation and precocious differentiation may contribute to club cell exhaustion, resulting in a decrease of club cells in the airway. Additionally, the loss of club cell *Cdh1* leads to increased type 2 cytokine expression and immune cell recruitment, including T cells, to the airways (Figure 5). While the loss of club cell *Cdh1* leads to major changes in the airway epithelium and microenvironment, the loss of ciliated cell *Cdh1* does not cause significant airway remodeling despite similar levels of inactivation.

When *Cdh1* mediated cell-cell contacts are lost specifically in club cells, the breakdown of epithelial cell communication leads to an increased localized immune response. In the *Scgb1a1*^{creERT}*; Cdh1*^{CKO} lung, many genes implicated in allergic airway inflammation and asthma are upregulated, including immune cell recruitment signals and pro-inflammatory cytokines. If E-CAD were only required for maintaining adherens

junctions and the airway barrier, we would expect to see a similar phenotype when *Cdh1* is inactivated in both club and ciliated cells due to a similar amount of barrier dysfunction. However, our findings reveal the loss of E-CAD adherens junctions is cell type dependent, and *Cdh1* plays a pivotal role in maintaining cell communication by differentially regulating airway epithelial homeostasis in a cell type specific manner. These results suggest that E-CAD may also function as a sensor of epithelial damage, and when club cells lose E-CAD, they initiate a dialogue with the immune system to recruit immune cells to the airways.

Club cells are an abundant progenitor population in the mouse airways and are necessary for maintaining the lung epithelium during normal aging and regeneration after lung injury [13]. There is increasing evidence that club cells are a heterogeneous population with subsets of club cells harboring higher progenitor potential [37,38]. Our study reveals insights into airway epithelial cell fate dynamics mediated by *Cdh1* and club cells. We find that airway epithelial proliferation and ciliated cell differentiation following loss of club cell *Cdh1* is robust and independent of IL4 and IL13 type 2 cytokine signaling. We also identify multiple mechanisms of achieving goblet cell metaplasia. In the absence of IL4 and IL13 signaling goblet cell differentiation is reduced but still present, suggesting there are mechanisms which rely on non – IL4 and IL13 mediated immune signaling. We also find that club to goblet cell differentiation can occur autonomously or non-autonomously after club cell loss of *Cdh1.* The non-autonomous signals influencing club to goblet cell fate could originate from *Cdh1* mutant club cells, immune cells, or other unknown pathways. The observance of mild goblet cell metaplasia after ciliated cell loss of *Cdh1* in the *Foxj1^{creERT2}; Cdh1^{CKO}* mutant, and

Cdh1+ club cells in our *Scgb1a1*^{creERT}; *Cdh1*^{CKO} mosaic analysis suggest that non-autonomous differentiation of club cells is a minor pathway to achieving goblet cell fate.

Club cells have a unique ability to metabolize toxins and regulate oxidative stress in the airway epithelium. We hypothesize that club cells may also play an active role in reducing inflammation in the airways, potentially by producing anti-inflammatory signals. A previous study demonstrated that the club cell secretoglobin *Scgb3a2* has anti-inflammatory activity, and *Scgb3a2* null mice display increased airway inflammation and inflammatory cytokine production following HDM allergen challenge [39]. *Pon1* is a regulator of oxidative stress and inflammation in the liver, and we identify *Pon1* as a potential club cell product. Following loss of *Cdh1* club cell markers including *Pon1* are reduced, and the depletion of club cells leads to increased production of cytokines and immune signals. *Pon1* may be an anti-inflammatory product of club cells, and future studies are needed to investigate the role of *Pon1* and other club cell products in regulating airway inflammation. Our study provides insight into the mechanisms through which the airway epithelium, particularly pulmonary club cells, protect the lung by participating in innate immune response and serving as the first line of defense.

Methods

Experimental model and subject details

Cdh1^{flox}, *Scgb1a1*^{creERT}, *Foxj1*^{creERT2}, *Rosa*^{Sun1GFP}, *Rosa*^{TdTom}, and *Il4Rα*$^{-/-}$ alleles and transgenic lines have been described previously [12–16,29]. Mice were housed and all experimental procedures were performed in an American Association for Accreditation of Laboratory Animal Care-accredited laboratory animal facility at the University of California San Diego (UCSD). *Cre* activity was induced by Tamoxifen administration by intraperitoneal injection. Tamoxifen was dissolved in corn oil and 25 mg of Tamoxifen was injected per gram of body weight. Tamoxifen was injected once per day for four consecutive days in 8 week old mice. For mosaic inactivation of *Scgb1a1*^{creERT}; *Cdh1*$^{flox/flox}$ mice, Tamoxifen was diluted and 0.25mg was injected once.

Tissue preparation and immunostaining

Lungs were inflated with 4% paraformaldehyde (Electron Microscopy Sciences) diluted in PBS, and fixed at 4C overnight. Samples were either embedded in paraffin or frozen in OCT (Electron Microscopy Sciences) for sectioning. Sections were immunostained using standard protocols. Slides were mounted with Fluoromount-G and visualized/photographed using a Zeiss AxioImager.A2 microscope and AxioCam MRc camera. Confocal images were acquired on a Leica Sp8 confocal microscope and camera. Images were processed using ImageJ.

Flow Cytometry

Lungs were inflated with dissociation buffer containing Collagenase D, Dispase, FBS, and RPMI and incubated at 37C shaking for 30 minutes. Following lung dissociation into a single cell suspension, red blood cells were lysed using ACK Lysis Buffer. Cells were stained with CD45-biotin and CD31-biotin conjugated antibodies then performed magnetic depletion of immune and endothelial cells from the cell mixture using streptavidin coated magnetic spheres (EasySep). Cells were then stained for Streptavidin BV510 to identify any remaining immune and endothelial cells, and CD326-APC to stain epithelial cells. Three mice per genotype (*Scgb1a1*^{creERT}*; Cdh1*$^{flox/+}$*; Rosa*^{Sun1GFP} and *Scgb1a1*^{creERT}*; Cdh1*$^{flox/flox}$*; Rosa*^{Sun1GFP}*)* were pooled together into one FACS sample. FACS data was analyzed using FlowJo software.

Quantitative RT-PCR (qRT-PCR)

RNA was isolated from whole lungs using an RNEasy mini kit (Qiagen) as per the manufacturer's protocol. 1000µg of RNA was reverse transcribed into cDNA using the iScript Reverse Transcriptase (Bio-Rad Laboratories). For qRT-PCR, 10ng of cDNA was amplified using gene-specific primers and iTaq SYBR green Supermix (Bio-Rad Laboratories) on a Bio-Rad CFX Connect real-time PCR machine. For each gene, at least three technical replicates and three biological replicates were assayed. Data were analyzed with the change in cycle threshold (Ct) value method. Statistical significance was determined using Student’s t-test. For a list of gene-specific primers, see Table S1.

RNA-seq analysis

Control and *Scgb1a1*^{creERT}*; Cdh1*^{CKO} lungs were dissected in PBS and immediately stored in TRIzol Reagent (ThermoFisher Scientific). Tissues were then lysed using a TissueLyser (Qiagen), and total mRNA was extracted using standard TRIzol RNA extraction protocol. mRNA was cleaned using the RNeasy Micro Kit (Qiagen). cDNA libraries were made for each individual lung or trachea using Illumina TruSeq RNA Library Prep Kit V2 (Illumina) and sequenced on a SR100 run on the HiSeq4000 platform (Illumina). Sequences in FASTQ files were aligned to the mouse reference genome using STAR [40]. Reads were counted using featureCounts and differential expression analysis was performed using DeSeq2 [41,42]. Volcano plot was generated using EnhancedVolcano R package [43]. Heatmap was generated using HeatMapper software [44].

Quantification and statistical analysis

Cell counts were quantified manually using the ImageJ Cell Counter feature. For each sample, six different sections from the same lung were quantified and the average was taken to represent the count for each sample. Statistical significance was determined using Student's t-test, and presented as mean ± standard deviation.

Acknowledgements

We thank the members of the Sun lab for insightful discussions. Confocal imaging was performed at the UCSD School of Medicine Microscopy Core, supported by NINDS NS047101. RNA-seq was conducted at the UCSD IGM Core. This work was supported by National Heart, Lung, and Blood Institute grants R01 HL142215, HL143256, HL122406 and HL119946 (to X.S.). R.Y. has received support from the NSF GRFP #DGE-1747503 and the Laboratory of Genetics at U.W. Madison NIH Training Grant #5T32GM007133.

Author Contributions

Conceptualization: R.E.Y., X.S.; Methodology: R.E.Y., L.B.N., X.S.; Validation: R.E.Y.; Formal analysis: R.E.Y.; Investigation: R.E.Y., L.B.M., B.D., J.B., J.M.V.; Resources: R.E.Y., X.S.; Data curation: R.E.Y.; Writing: R.E.Y., X.S.; Visualization: R.E.Y., X.S.; Supervision: X.S.; Project administration: X.S.; Funding acquisition: R.E.Y., X.S.

References

1. Georas SN, Rezaee F. Epithelial barrier function: At the front line of asthma immunology and allergic airway inflammation. *J Allergy Clin Immunol*. 2014;134(3):509-520. doi:10.1016/j.jaci.2014.05.049
2. Heijink IH, Nawijn MC, Hackett TL. Airway epithelial barrier function regulates the pathogenesis of allergic asthma. *Clin Exp Allergy*. 2014;44(5):620-630. doi:10.1111/cea.12296
3. Nawijn MC, Hackett TL, Postma DS, van Oosterhout AJM, Heijink IH. E-cadherin: Gatekeeper of airway mucosa and allergic sensitization. *Trends Immunol*. 2011;32(6):248-255. doi:10.1016/j.it.2011.03.004
4. Hackett T-L, de Bruin HG, Shaheen F, et al. Caveolin-1 Controls Airway Epithelial Barrier Function. Implications for Asthma. *Am J Respir Cell Mol Biol*. 2013;49(4):662-671. doi:10.1165/rcmb.2013-0124OC
5. Goto Y. Dislocation_Ecadherin_astmatic_response_2000.pdf. *Am J Respir Cell Mol Biol*. 2000;23:712-718.
6. Kim HT, Yin W, Nakamichi Y, et al. WNT/RYK signaling restricts goblet cell differentiation during lung development and repair. *Proc Natl Acad Sci U S A*. 2019;116(51):25697-25706. doi:10.1073/pnas.1911071116
7. Danahay H, Pessotti AD, Coote J, et al. Notch2 is required for inflammatory cytokine-driven goblet cell metaplasia in the lung. *Cell Rep*. 2015;10(2):239-252. doi:10.1016/j.celrep.2014.12.017
8. Gour N, Wills-Karp M. IL-4 and IL-13 signaling in allergic airway disease. *Cytokine*. 2015;75(1):68-78. doi:10.1016/j.cyto.2015.05.014

9. Waddell A, Vallance JE, Hummel A, Alenghat T, Rosen MJ. IL-33 Induces Murine Intestinal Goblet Cell Differentiation Indirectly via Innate Lymphoid Cell IL-13 Secretion. *J Immunol*. 2019;202(2):598-607. doi:10.4049/jimmunol.1800292

10. Kondo Y, Yoshimoto T, Yasuda K, et al. Administration of IL-33 induces airway hyperresponsiveness and goblet cell hyperplasia in the lungs in the absence of adaptive immune system. *Int Immunol*. 2008;20(6):791-800. doi:10.1093/intimm/dxn037

11. Rajavelu P, Chen G, Xu Y, Kitzmiller JA, Korfhagen TR, Whitsett JA. Airway epithelial SPDEF integrates goblet cell differentiation and pulmonary Th2 inflammation. *J Clin Invest*. 2015;125(5):2021-2031. doi:10.1172/JCI79422

12. Boussadia O, Kutsch S, Hierholzer A, Delmas V, Kemler R. E-cadherin is a survival factor for the lactating mouse mammary gland. *Mech Dev*. 2002;115(1-2):53-62. doi:10.1016/S0925-4773(02)00090-4

13. Rawlins EL, Okubo T, Xue Y, et al. The Role of Scgb1a1+ Clara Cells in the Long-Term Maintenance and Repair of Lung Airway, but Not Alveolar, Epithelium. *Cell Stem Cell*. 2009;4(6):525-534. doi:10.1016/j.stem.2009.04.002

14. Rawlins EL, Ostrowski LE, Randell SH, Hogan BLM. Lung development and repair: Contribution of the ciliated lineage. *Proc Natl Acad Sci U S A*. 2007;104(2):410-417. doi:10.1073/pnas.0610770104

15. Mo A, Mukamel EA, Davis FP, et al. Epigenomic Signatures of Neuronal Diversity in the Mammalian Brain. *Neuron*. 2015;86(6):1369-1384. doi:10.1016/j.neuron.2015.05.018

16. Madisen L, Zwingman TA, Sunkin SM, et al. A robust and high-throughput Cre

Repooting and characterization. *Nat Neurosci*. 2010;13(1):133-140. doi:10.1038/nn.2467.A

17. Oeser K, Maxeiner J, Symowski C, Stassen M, Voehringer D. T cells are the critical source of IL-4/IL-13 in a mouse model of allergic asthma. *Allergy Eur J Allergy Clin Immunol*. 2015;70(11):1440-1449. doi:10.1111/all.12705
18. Hwang JY, Randall TD, Silva-Sanchez A. Inducible bronchus-associated lymphoid tissue: Taming inflammation in the lung. *Front Immunol*. 2016;7(JUN):1-17. doi:10.3389/fimmu.2016.00258
19. Shunmoogam N, Naidoo P, Chilton R. Paraoxonase (PON)-1: A brief overview on genetics, structure, polymorphisms and clinical relevance. *Vasc Health Risk Manag*. 2018;14:137-143. doi:10.2147/VHRM.S165173
20. Rumora L, Rajković MG, Kopčinović LM, Pancirov D, Čepelak I, Grubišić TŽ. Paraoxonase 1 activity in patients with chronic obstructive pulmonary disease. *COPD J Chronic Obstr Pulm Dis*. 2014;11(5):539-545. doi:10.3109/15412555.2014.898028
21. Rajković MG, Popović-Grle S, Dugac AV, et al. PON1 gene polymorphisms in patients with chronic obstructive pulmonary disease. *J Clin Pathol*. 2018;71(11):963-970. doi:10.1136/jclinpath-2018-205194
22. Sarioglu N, Bilen C, Cevik C, Gencer N. Paraoxonase activity and phenotype distribution in patients with chronic obstructive pulmonary disease. *Eurasian J Med*. 2020;52(2):161-165. doi:10.5152/eurasianjmed.2019.19122
23. Rodrigo L, Hernández AF, López-Caballero JJ, Gil F, Pla A. Immunohistochemical evidence for the expression and induction of paraoxonase

in rat liver, kidney, lung and brain tissue. Implications for its physiological role. *Chem Biol Interact*. 2001;137(2):123-137. doi:10.1016/S0009-2797(01)00225-3

24. Tölgyesi G, Molnár V, Semsei ÁF, et al. Gene expression profiling of experimental asthma reveals a possible role of paraoxonase-1 in the disease. *Int Immunol*. 2009;21(8):967-975. doi:10.1093/intimm/dxp063
25. Emin O, Hasan A, Rusen DM. Plasma paraoxonase, oxidative status level, and their relationship with asthma control test in children with asthma. *Allergol Immunopathol (Madr)*. 2015;43(4):346-352. doi:10.1016/j.aller.2014.05.009
26. Chen W, Chen Y, Xiang ZX, Zhao WJ, Hu Q. Influences of PON1 on airway inflammation and remodeling in bronchial asthma. 2018;(April 2017):793-805. doi:10.1002/jcb.26242
27. Grünig G, Warnock M, Wakil AE, et al. NIH Public Access. 2014;282(5397):2261-2263.
28. Kuperman DA, Huang X, Nguyenvu L, Hölscher C, Brombacher F, Erle DJ. IL-4 Receptor Signaling in Clara Cells Is Required for Allergen-Induced Mucus Production. *J Immunol*. 2005;175(6):3746-3752. doi:10.4049/jimmunol.175.6.3746
29. Noben-Trauth N, Shultz LD, Brombacher F, Urban JF, Gu H, Paul WE. An interleukin 4 (IL-4)-independent pathway for CD4+ T cell IL-4 production is revealed in IL-4 receptor-deficient mice. *Proc Natl Acad Sci U S A*. 1997;94(20):10838-10843. doi:10.1073/pnas.94.20.10838
30. Heijink IH, Kies PM, Kauffman HF, Postma DS, van Oosterhout AJM, Vellenga E. Down-Regulation of E-Cadherin in Human Bronchial Epithelial Cells Leads to Epidermal Growth Factor Receptor-Dependent Th2 Cell-Promoting Activity. *J*

Immunol. 2007;178(12):7678-7685. doi:10.4049/jimmunol.178.12.7678

31. Ierodiakonou D, Postma DS, Koppelman GH, et al. E-cadherin gene polymorphisms in asthma patients using inhaled corticosteroids. 2011;38(5):1044-1052. doi:10.1183/09031936.00194710
32. Heijink IH, van Oosterhout A, Kapus A. Epidermal growth factor receptor signalling contributes to house dust mite-induced epithelial barrier dysfunction. *Eur Respir J*. 2010;36(5):1016-1026. doi:10.1183/09031936.00125809
33. Heijink IH, Postma DS, Noordhoek JA, Broekema M, Kapus A. House Dust Mite–Promoted Epithelial-to-Mesenchymal Transition in Human Bronchial Epithelium. *Am J Respir Cell Mol Biol*. 2010;42(1):69-79. doi:10.1165/rcmb.2008-0449OC
34. Bruner HC, Derksen PWB. Adhesion and the Development and Progression of Cancer. 2020;3(Table 1).
35. Post S, Heijink IH, Hesse L, et al. Characterization of a lung epithelium specific E-cadherin knock-out model: Implications for obstructive lung pathology. *Sci Rep*. 2018;8(1):1-12. doi:10.1038/s41598-018-31500-8
36. Ceteci F, Ceteci S, Zanucco E, et al. E-cadherin controls bronchiolar progenitor cells and onset of preneoplastic lesions in mice. *Neoplasia (United States)*. 2012;14(12):1164-1177. doi:10.1593/neo.121088
37. Kathiriya JJ, Brumwell AN, Jackson JR, Tang X, Chapman HA. Distinct Airway Epithelial Stem Cells Hide among Club Cells but Mobilize to Promote Alveolar Regeneration. *Cell Stem Cell*. 2020;26(3):346-358.e4. doi:10.1016/j.stem.2019.12.014
38. Strunz M, Simon LM, Ansari M, et al. Alveolar regeneration through a Krt8+

transitional stem cell state that persists in human lung fibrosis. *Nat Commun*. 2020;11(1). doi:10.1038/s41467-020-17358-3

39. Yoneda M, Xu L, Kajiyama H, et al. Secretoglobin superfamily protein SCGB3A2 alleviates house dust mite-induced allergic airway inflammation in mice. *Int Arch Allergy Immunol*. 2016;171(1):36-44. doi:10.1159/000450788
40. Dobin A, Davis CA, Schlesinger F, et al. STAR: Ultrafast universal RNA-seq aligner. *Bioinformatics*. 2013;29(1):15-21. doi:10.1093/bioinformatics/bts635
41. Liao Y, Smyth GK, Shi W. FeatureCounts: An efficient general purpose program for assigning sequence reads to genomic features. *Bioinformatics*. 2014;30(7):923-930. doi:10.1093/bioinformatics/btt656
42. Love MI, Huber W, Anders S. Moderated estimation of fold change and dispersion for RNA-seq data with DESeq2. *Genome Biol*. 2014;15(12):1-21. doi:10.1186/s13059-014-0550-8
43. Blighe K, Rana S, Lewis M. EnhancedVolcano: Publication-ready volcano plots with enhanced colouring and labeling. 2020.
44. Babicki S, Arndt D, Marcu A, et al. Heatmapper: web-enabled heat mapping for all. *Nucleic Acids Res*. 2016;44(W1):W147-W153. doi:10.1093/nar/gkw419

Figures

Figure 1
Young et al.

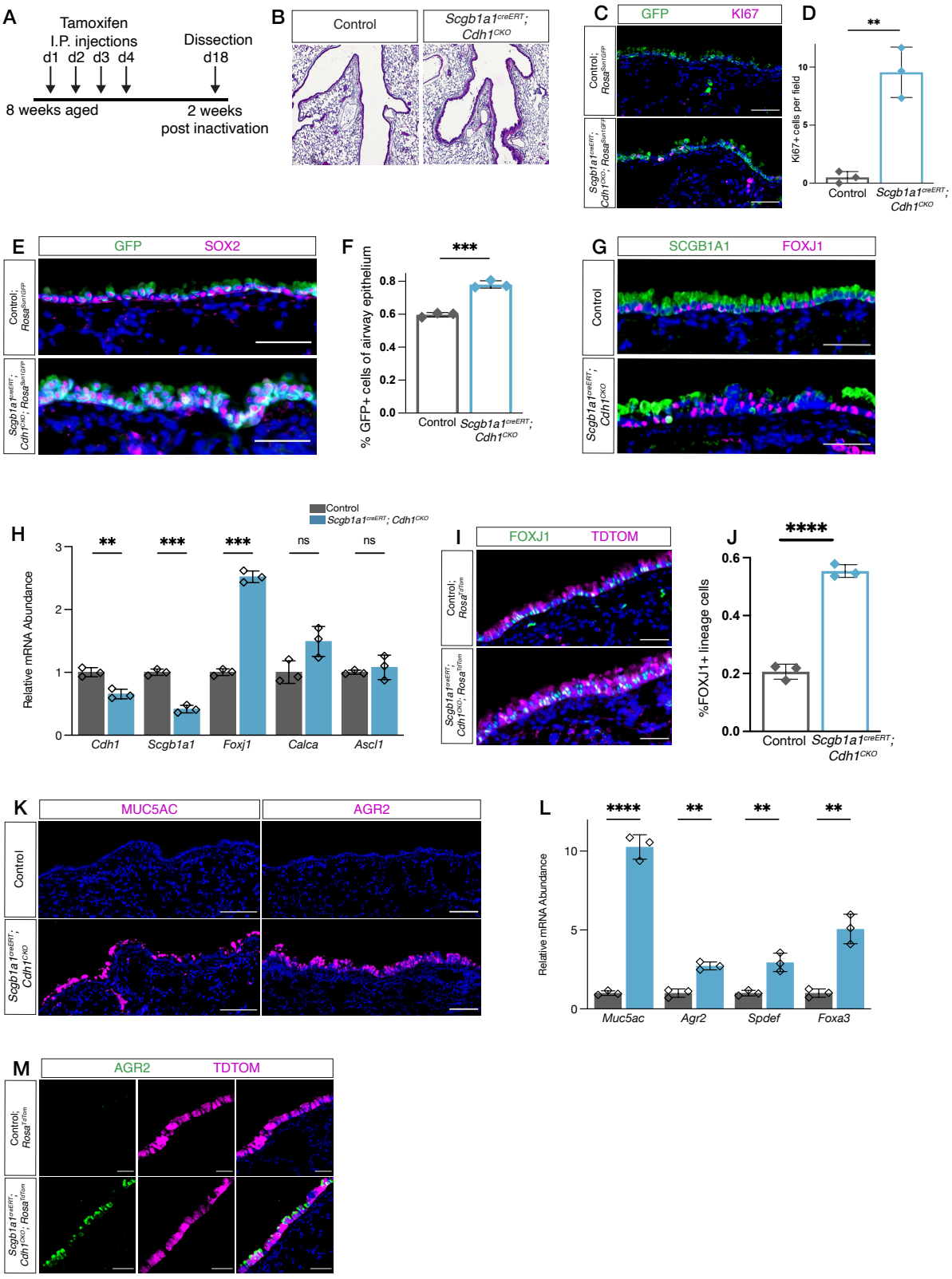

Figure 1: Inactivation of *Cdh1* in pulmonary club cells leads to increased epithelial proliferation, ciliated and goblet cell differentiation.

A) Timeline of Tamoxifen injections and analysis for *Scgb1a1^{creERT}; Cdh1^{CKO}* and *Foxj1^{creERT2}; Cdh1^{CKO}* mice. B) H&E staining depicting airway thickening in the *Scgb1a1^{creERT}; Cdh1^{CKO}* lung. C) Confocal images showing immunofluorescent detection of GFP (green) and proliferation marker Ki67 (magenta) in airways of control and *Scgb1a1^{creERT}; Cdh1^{CKO}* mice, Scalebar: 50 μm. D) Quantification of proliferative Ki67+ airway epithelial cells in control and *Scgb1a1^{creERT}; Cdh1^{CKO}* lung per microscopic field, N=3 each. Data are represented as individual points for each biological sample ± SD. E) Immunofluorescent detection of GFP (green) and pan airway epithelial marker SOX2 (magenta) expression in airways of control and *Scgb1a1^{creERT}; Cdh1^{CKO}* lung, Scalebar: 50 μm. F) Quantification of labelled GFP+ per total SOX2+ airway epithelial cells in control and *Scgb1a1^{creERT}; Cdh1^{CKO}* lung, N=3 each. Data are represented as individual points for each biological sample ± SD. G) Immunofluorescent detection of SCGB1A1 club cells (green) and FOXJ1 ciliated cells (magenta) in airways of control and *Scgb1a1^{creERT}; Cdh1^{CKO}* lung, Scalebar: 50 μm. H) qRT-PCR quantification of relative mRNA levels of *Cdh1, Scgb1a1, Foxj1, Calca,* and *Ascl1* in control and *Scgb1a1^{creERT}; Cdh1^{CKO}* lungs. Data are represented as individual points for each biological sample ± SD. ns: not significant, **: $p<0.005$, ***: $p<0.0005$. I) Immunofluorescent detection of FOXJ1 ciliated cells (green) and TDTOM+ lineage cells (magenta) in airways of control and *Scgb1a1^{creERT}; Cdh1^{CKO}* lung, Scalebar: 50 μm. J) Quantification of TDTOM+ lineage labelled FOXJ1 ciliated cells per total FOXJ1 ciliated cells in control and *Scgb1a1^{creERT}; Cdh1^{CKO}* lung per microscopic field, N=3 each. Data

are represented as individual points for each biological sample ± SD. K) Confocal images showing immunofluorescent detection of goblet cell markers MUC5AC (magenta; left panels) and AGR2 (magenta; right panels) in airways of control and *Scgb1a1*^{creERT}*; Cdh1*^{CKO} mice, Scalebar: 100 μm. L) qRT-PCR quantification of relative mRNA levels of *Muc5ac, Agr2, Spdef,* and *Foxa3* in control and *Scgb1a1*^{creERT}*; Cdh1*^{CKO} lungs. Data are represented as individual points for each biological sample ± SD. **: $p<0.005$, ****: $p<0.00005$. M) Confocal images showing immunofluorescent detection of AGR2 (green) and TDTOM lineage label (magenta) in airways of control and *Scgb1a1*^{creERT}*; Cdh1*^{CKO} mice, Scalebar: 50 μm.

Figure 2
Young et al.

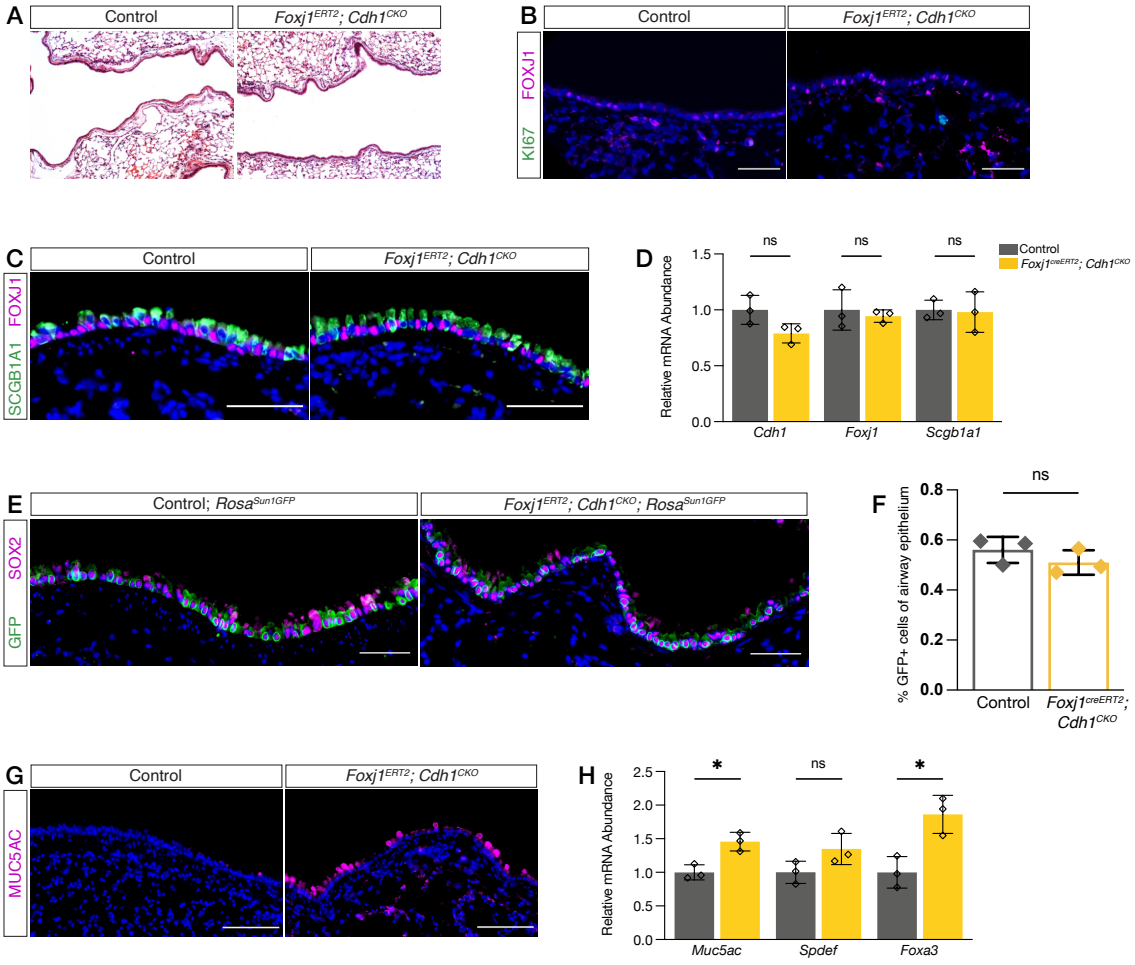

Figure 2: *Cdh1* inactivation in ciliated cells does not cause airway remodeling

A) H&E staining of control and *Foxj1^{creERT2}; Cdh1^{CKO}* lung. B) Immunofluorescent detection of proliferation marker KI67 (green) and ciliated cell marker FOXJ1 (magenta) in airways of control and *Foxj1^{creERT2}; Cdh1^{CKO}* mice, Scalebar: 50 μm. C) Immunofluorescent detection of club cell SCGB1A1 (green) and ciliated cell FOXJ1 (magenta) in airways of control and *Foxj1^{creERT2}; Cdh1^{CKO}* mice, Scalebar: 50 μm. D) qRT-PCR quantification of relative mRNA levels of *Cdh1, Foxj1,* and *Scgb1a1* in control and *Foxj1^{creERT2}; Cdh1^{CKO}* lungs. Data are represented as individual points for each biological sample ± SD. ns: not significant, ns: not significant. E) Immunofluorescent detection of GFP (green) and pan airway epithelial marker SOX2 (magenta) expression in airways of control and *Foxj1^{creERT2}; Cdh1^{CKO}* lung, Scalebar: 50 μm. F) Quantification of labelled GFP+ per total SOX2+ airway epithelial cells in control and *Foxj1^{creERT2}; Cdh1^{CKO}* lung, N=3 each. Data are represented as individual points for each biological sample ± SD. G) Immunofluorescent detection of goblet cell marker MUC5AC (magenta) in airways of control and *Foxj1^{creERT2}; Cdh1^{CKO}* mice, Scalebar: 50 μm. L) qRT-PCR quantification of relative mRNA levels of *Muc5ac, Spdef,* and *Foxa3* in control and *Foxj1^{creERT2}; Cdh1^{CKO}* lungs. Data are represented as individual points for each biological sample ± SD. ns: not significant, *: $p<0.05$.

Figure 3
Young et al.

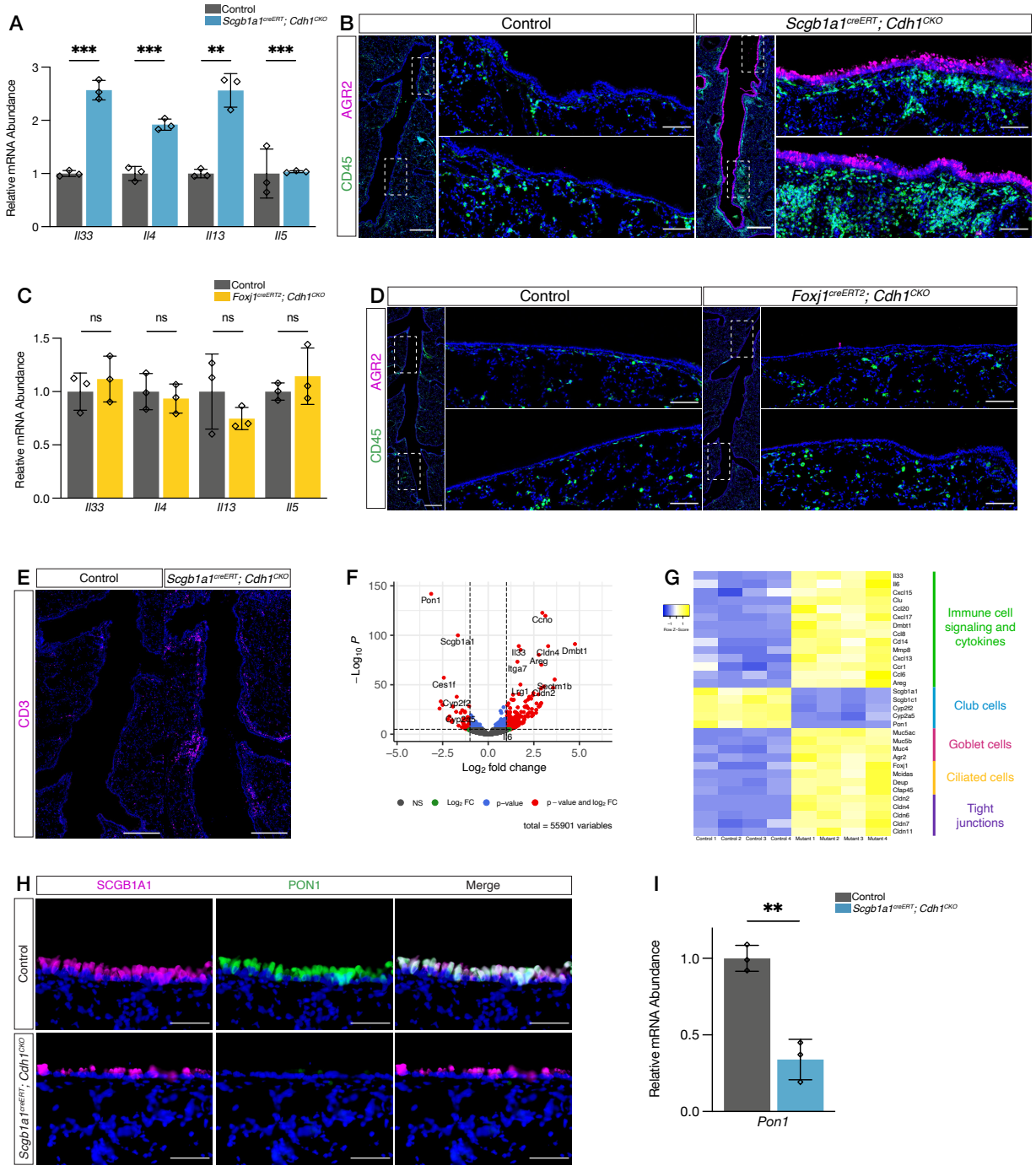

Figure 3: Loss of club cell *Cdh1* leads to changes in immune signature including increase type 2 cytokines and immune cell recruitment

A) qRT-PCR quantification of relative mRNA levels of *Il33, Il4, Il13,* and *Il5* in control and *Scgb1a1^{creERT}; Cdh1^{CKO}* lungs. Data are represented as individual points for each biological sample ± SD. ns: not significant, ns: not significant, **: p<0.005, ***: p<0.0005. B) Maximum projection of z-stacks from confocal images showing immunofluorescent detection of pan neuronal marker CD45 (green) and goblet cell marker AGR2 (magenta) in airways of control and *Scgb1a1^{creERT}; Cdh1^{CKO}* mice, Scalebar: 500 μm. Inset panels, Scalebar: 100 μm. C) qRT-PCR quantification of relative mRNA levels of *Il33, Il4, Il13,* and *Il5* in control and *Foxj1^{creERT2}; Cdh1^{CKO}* lungs. Data are represented as individual points for each biological sample ± SD. ns: not significant, ns: not significant. D) Maximum projection of z-stacks from confocal images showing immunofluorescent detection of pan neuronal marker CD45 (green) and goblet cell marker AGR2 (magenta) in airways of control and *Foxj1^{creERT2}; Cdh1^{CKO}* mice, Scalebar: 500 μm. Inset panels, Scalebar: 100 μm. E) Maximum projection of z-stacks from confocal images showing immunofluorescent detection of global T cell marker CD3 (magenta) in airways of control and *Scgb1a1^{creERT}; Cdh1^{CKO}* mice, Scalebar: 300 μm. F) Volcano plot displaying differentially expressed genes in bulk RNA-seq dataset between control and *Scgb1a1^{creERT}; Cdh1^{CKO}* lungs. G) Heatmap of RNA-seq data showing groups of significantly upregulated (yellow) and downregulated (blue) genes, by an adjusted p-value less than 0.05, in the *Scgb1a1^{creERT}; Cdh1^{CKO}* lungs. H) Immunofluorescent detection of club cell marker SCGB1A1 (magenta) and PON1 (green) expression in airways of control and *Scgb1a1^{creERT}; Cdh1^{CKO}* mice, Scalebar:

50 μm. l) qRT-PCR quantification of relative mRNA levels of *Pon1* in control and *Scgb1a1*^{creERT}*; Cdh1*^{CKO} lungs. Data are represented as individual points for each biological sample ± SD. ns: not significant, **: p<0.005.

Figure 4
Young et al.

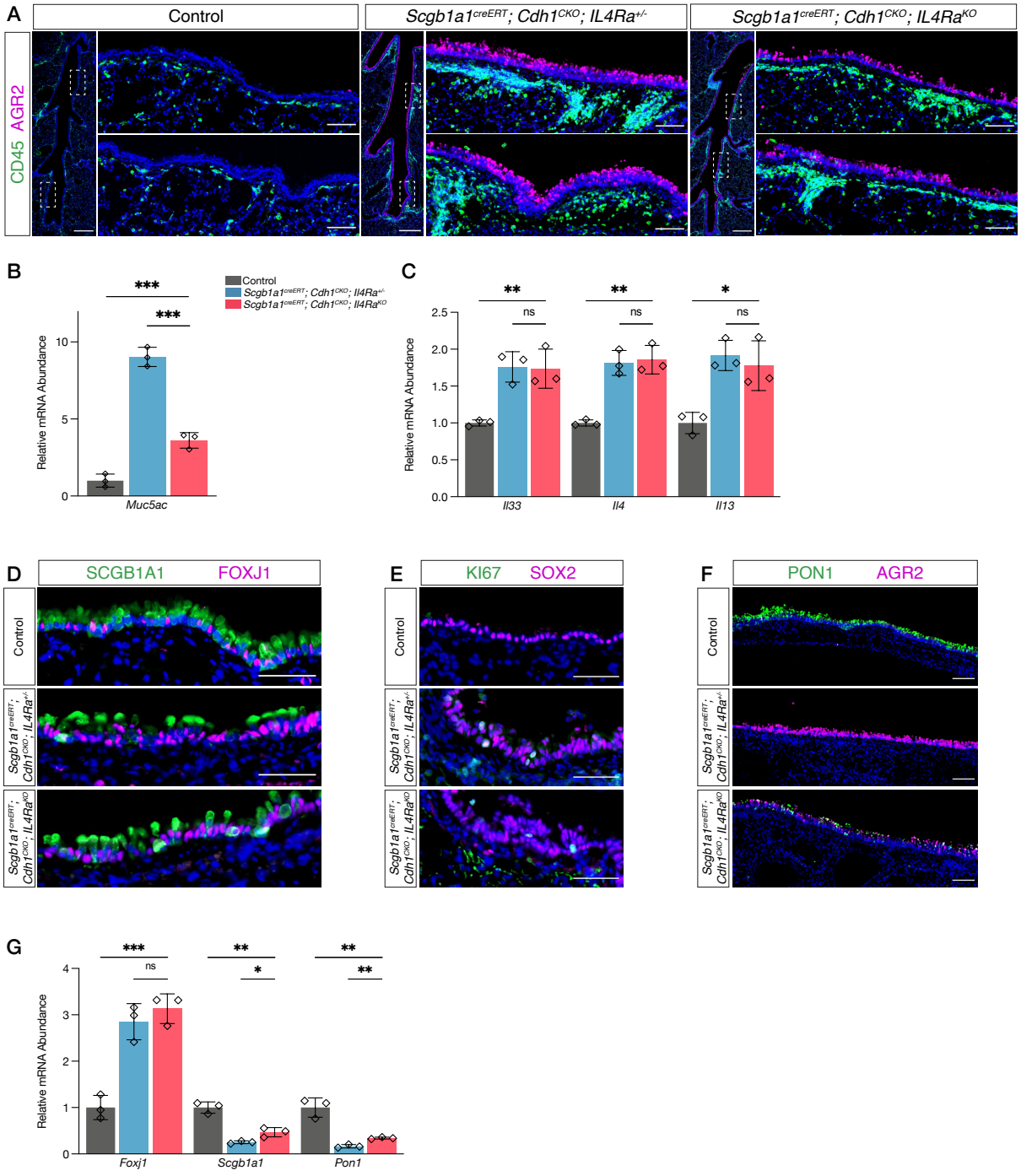

Figure 4: Goblet cell metaplasia is partially dependent on type 2 immune signaling

A) Maximum projection of z-stacks from confocal images showing immunofluorescent detection of pan neuronal marker CD45 (green) and goblet cell marker AGR2 (magenta) in airways of control, *Scgb1a1^{creERT}; Cdh1^{CKO}*; *Il4Rα$^{+/-}$* (single mutant), and *Scgb1a1^{creERT}; Cdh1^{CKO}*; *Il4Rα^{KO}* (double mutant) mice, Scalebar: 500 μm. Inset panels, Scalebar: 100 μm. B) qRT-PCR quantification of relative mRNA levels of *Muc5ac* in control, *Scgb1a1^{creERT}; Cdh1^{CKO}*; *Il4Rα$^{+/-}$*, and *Scgb1a1^{creERT}; Cdh1^{CKO}*; *Il4Rα^{KO}* lungs. Data are represented as individual points for each biological sample ± SD. ***: p<0.0005. C) qRT-PCR quantification of relative mRNA levels of *Il33, Il4,* and *Il13* in control, *Scgb1a1^{creERT}; Cdh1^{CKO}*; *Il4Rα$^{+/-}$*, and *Scgb1a1^{creERT}; Cdh1^{CKO}*; *Il4Rα^{KO}* lungs. Data are represented as individual points for each biological sample ± SD. ns: not significant, *: p<0.05, **: p<0.005. D) Immunofluorescent detection of club cell marker SCGB1A1 (green) and ciliated cell marker FOXJ1 (magenta), Scalebar: 50 μm. E) Immunofluorescent detection of proliferation marker KI67 (green) and airway epithelial marker SOX2 (magenta), Scalebar: 50 μm. F) Maximum projection of z-stacks from confocal images showing immunofluorescent detection of PON1 (green) and goblet cell marker AGR2 (magenta), Scalebar: 100 μm. G) qRT-PCR quantification of relative mRNA levels of *Foxj1, Scgb1a1,* and *Pon1* in control, *Scgb1a1^{creERT}; Cdh1^{CKO}*; *Il4Rα$^{+/-}$*, and *Scgb1a1^{creERT}; Cdh1^{CKO}*; *Il4Rα^{KO}* lungs. Data are represented as individual points for each biological sample ± SD. ns: not significant, *: p<0.05, **: p<0.005, ***: p<0.005.

Figure 5
Young et al.

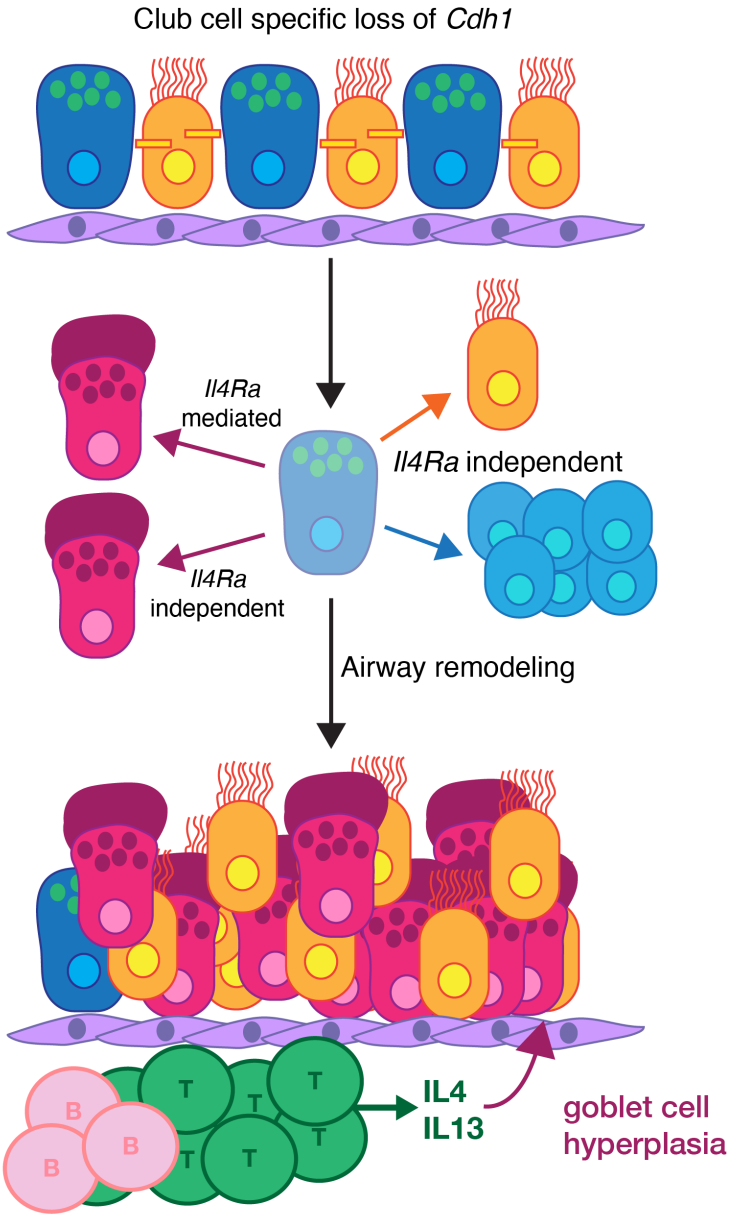

Figure 5: Summary diagram.

Supplemental Figure 1
Young et al.

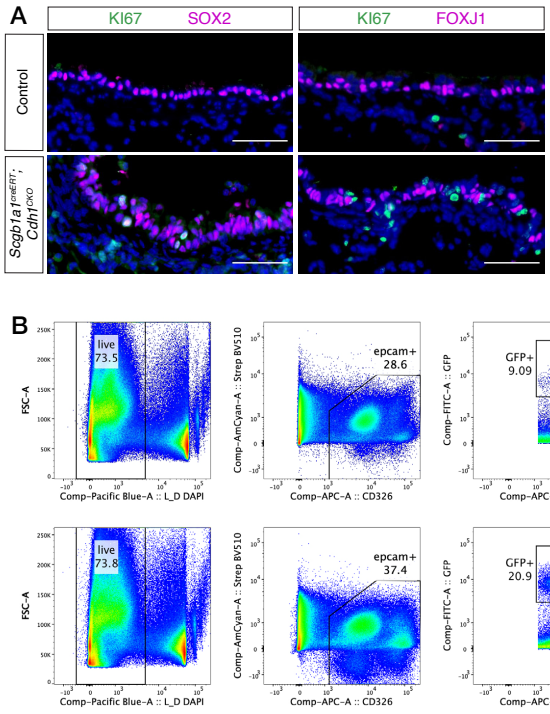

Supplemental Figure 1

A) Immunofluorescent detection of proliferation marker KI67 (green), airway epithelial marker SOX2 (magenta, left), and ciliated cell marker FOXJ1 (magenta, right) in control and *Scgb1a1*^{creERT}*; Cdh1*^{CKO} lungs Scalebar: 50 μm. B) Dot plots of FACS data depicting gating strategy for sorting live cells (DAPI negative) > CD45 and CD31 negative cells (Streptavidin BV510 negative) > Epcam cells (APC positive) > GFP positive cells. C) Quantification summary of FACS data depicting the GFP positive cells as the percentage of total Epcam positive cells. Data are represented as individual points for each individual FACS sample $\pm$ SD. **: $p<0.005$

Supplemental Figure 2
Young et al.

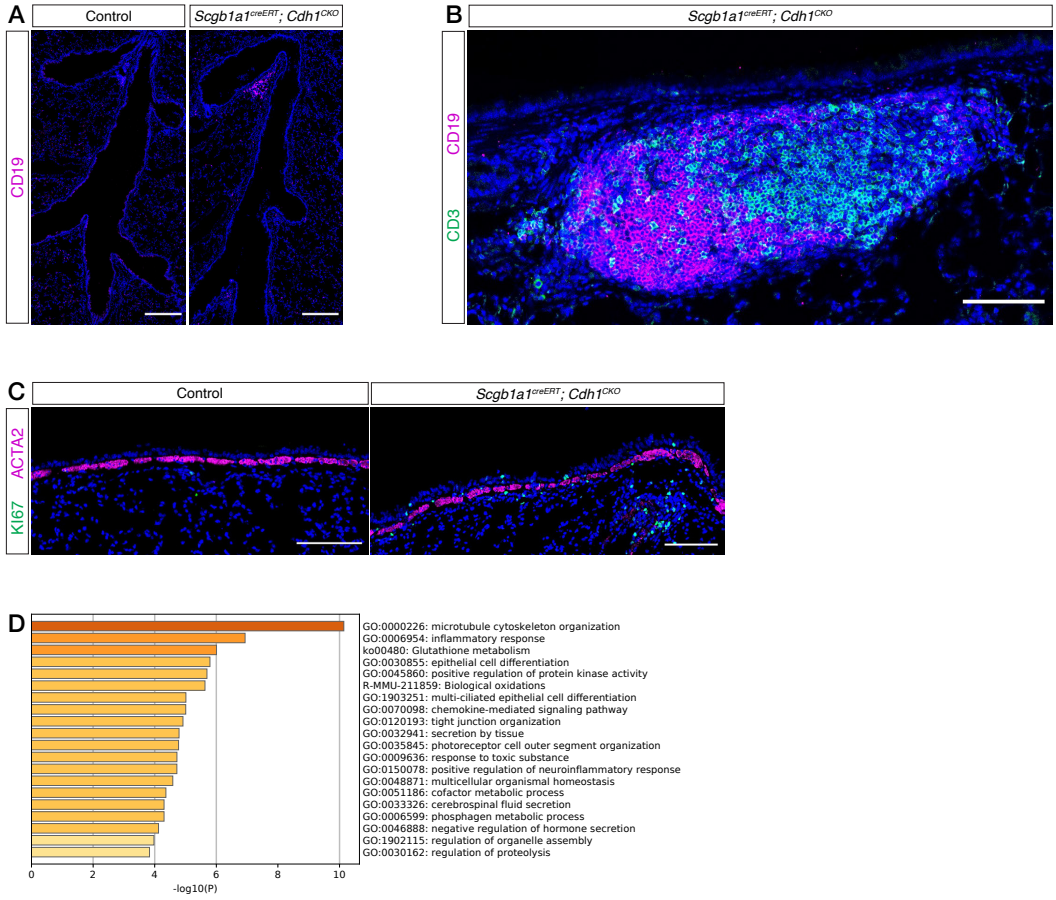

Supplemental Figure 2

A) Maximum projection of z-stacks from confocal images showing immunofluorescent detection of B cell marker CD19 (magenta) in control and *Scgb1a1*^{creERT}*; Cdh1*^{CKO} lungs, Scalebar: 300 µm. B) Immunofluorescent detection of T cell marker CD3 (green) and B cell marker CD19 (magenta) in control and *Scgb1a1*^{creERT}*; Cdh1*^{CKO} lungs, Scalebar: 100 µm. C) Immunofluorescent detection of proliferation marker KI67 (green) and airway smooth muscle marker ACTA2 (magenta) in control and *Scgb1a1*^{creERT}*; Cdh1*^{CKO} lungs, Scalebar: 100 µm. D) GO-Term analysis for significantly differentially expressed genes in RNA-seq data of control and *Scgb1a1*^{creERT}*; Cdh1*^{CKO} lungs.

Supplemental Figure 3
Young et al.

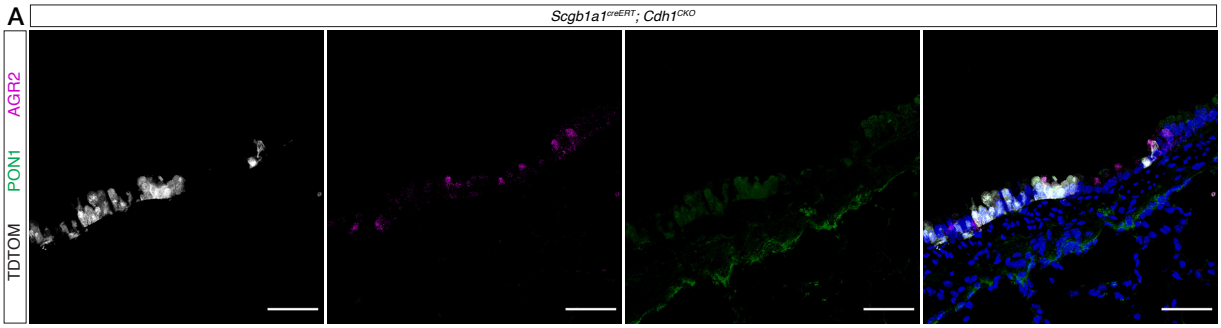

Supplemental Figure 3

A) Immunofluorescent detection of lineage labelled TDTOM cells (white), goblet cell marker AGR2 (magenta), and PON1 (green) in *Scgb1a1*^{creERT}*; Cdh1*^{CKO} mosaic inactivation lungs, Scalebar: 50 μm.

Concluding statement

In my dissertation, I have uncovered novel mechanisms underlying tissue crosstalk during lung development and disease. During development, airway smooth muscle plays a multi-faceted role by establishing tracheal architecture and promoting airway epithelial growth. We reveal a potential mechanism of BMP signaling in regulating airway size, however future work will be needed to validate these findings potentially by specific mesenchymal and epithelial knock-outs of BMP ligands and receptors. Contrary to the prevailing dogma in the field, we found that differentiation of airway smooth muscle is not necessary for proper lung epithelial branching. This unexpected finding highlights the power of in vivo genetic models in addressing complex biological questions. In addition to focusing on one mesenchymal cell type, it will be of interest to uncover the diversity of the lung mesenchyme. Compared to other tissues, especially the epithelium, the heterogeneity of the mesenchyme, how mesenchymal cell fates are initiated during development and maintained during homeostasis, and the role of the mesenchyme in establishing lung architecture and regulating homeostasis is largely unknown.

I also uncovered a novel role for *E-cadherin* in maintaining airway homeostasis and immune cell recruitment. This study reveals how the airway epithelium elicits an immune response to environmental insults. The role of club cells in metabolizing toxins has been implicated, but little is understood on the genetic mechanisms behind this process. Understanding how club cells combat environmental threats, potentially by regulating oxidative stress, will provide exciting insight on how club cells regulate airway homeostasis. Additionally, uncovering the specific epithelial signals that promote

immune response will be of high interest for future studies. Revealing the molecular crosstalk between the epithelium and immune system highlights the importance of epithelial barrier biology, and in the future may lead to novel treatments for barrier diseases, including asthma.

In summary, I have investigated mesenchymal-epithelial interactions that regulate lung and trachea development, and the importance of *E-cadherin* and airway club cells during epithelial-immune crosstalk in maintaining lung homeostasis. These findings shed light on how proper communication between different compartments of the lung is essential for building a functional tissue, and also required to maintain health as an adult. The airways are a major site of pathogenesis for many lung diseases of which few treatments and effective cures are available. By understanding the molecular and genetic mechanisms involved in pediatric and adult lung diseases, we can hopefully be a step closer to helping patients.